Article

SOURCE DATA | TRANSPARENT PROCESS | OPEN ACCESS | CHECK FOR UPDATES

THE EMBO JOURNAL

Tetraspanin CD81 restricts Ebola virus infection and is antagonized by glycoprotein GP and matrix protein VP40

Dan Hu[1,7], Elena Hagelauer[1,7], Lisa Wendt[2,6], Matteo Bosso[1], Maximilian Bunz[1], Julia Kammerloher[1,3], Jasmin S Kutter[3], Johannes Brandi[4], Lina Widerspick[1,4,5], Thomas Hoenen[2] & Michael Schindler[1,3]✉

Abstract

Viruses manipulate host cell membranes to evade antiviral immunity, prevent superinfection, and optimize their replication and spread. The Ebola virus glycoprotein GP mediates viral entry but also contributes to the subversion of host antiviral immune responses. Here, we characterize the impact of Ebola virus GP on cell surface proteins and show that it reduces cell surface availability of tetraspanins CD81, CD63, and CD9. This function is conserved among several filoviral glycoproteins but not observed for glycoproteins of other viral families. Whereas CD63 and CD9 are largely dispensable for Ebola virus replication, CD81 suppresses virus-like particle entry and viral replication. This activity might be attributed to CD81-mediated suppression of NF-κB signaling, which is induced by the Ebola virus matrix protein VP40 and transcription- and replication-competent virus-like particle (trVLP) replication. Our results further indicate that both GP, which interacts directly with CD81, and VP40, which also associates with CD81, function to reduce total and surface expression levels of CD81. CD81 is shown to reduce levels of Ebola virus RNA species, and its antibody-mediated clustering can suppress Ebola virus infection. Our study provides insights into the roles of NF-κB signaling in Ebola virus replication and immunopathogenesis, and identifies tetraspanin CD81 as a potentially druggable Ebola virus-inhibitory host factor.

Subject Categories Immunology; Microbiology, Virology & Host Pathogen Interaction

https://doi.org/10.1038/s44318-026-00940-8

Received 30 March 2026; Revised 17 August 2026;
Accepted 11 September 2026

Published online: 04 November 2026

Introduction

Ebola virus (EBOV), a member of the *Filoviridae* family, causes Ebola virus disease (EVD) in humans, with case fatalities from 40 to 60% (Kuhn et al, 2019a; Kuhn et al, 2019b; WHO, 2023a). Other members of the *Filoviridae* including Marburg virus (MARV), Sudan virus (SUDV), and Bundibugyo virus (BDBV) are also known to be highly fatal to humans (Kuhn et al, 2019b; WHO, 2023b). EBOV is filamentous in shape and enveloped with a membrane derived from the host cell plasma membrane (Beniac et al, 2012). A wide range of cell types can be infected by EBOV, such as macrophages, dendritic cells, hepatocytes, endothelial cells and epithelial cells (Feldmann and Geisbert, 2011).

One major driver of EVD pathogenesis is the excessive release of pro-inflammatory cytokines and chemokines (Baize et al, 2002; Reynard et al, 2019), which can be triggered by the viral glycoprotein (GP) in its full-length or shed form through binding to Toll-like receptor 4 and subsequent activation of the nuclear factor kappa B (NF-kB) pathway (Escudero-Perez et al, 2014; Okumura et al, 2010). Recently, it was also shown that the viral matrix protein VP40 can activate pro-inflammatory signaling via NF-kB, possibly involving tumor necrosis factor receptor 1 (TNFR1), although the exact mechanism remains unclear (Yamaoka et al, 2026).

For cell entry, EBOV can bind to a number of attachment factors via its surface glycoprotein (GP) and phosphatidylserine (PtdSer), which is embedded in the viral envelope (Moller-Tank and Maury, 2015). Identified attachment factors include the C-type lectins DC-SIGN, L-SIGN, hMGL, LSECtin, and MBL (Alvarez et al, 2002; Brudner et al, 2013; Moller-Tank and Maury, 2015; Powlesland et al, 2008; Takada et al, 2004). Furthermore, the PtdSer receptors Tim1, Tim4, and Tyro3 receptor tyrosine kinases (Axl, Dtk, and Mer) can facilitate attachment (Jemielity et al, 2013; Kondratowicz et al, 2011; Moller-Tank and Maury, 2015; Shimojima et al, 2006; Yuan et al, 2015). Cell-based assays demonstrate that following attachment, EBOV is internalized

[1]Institute for Medical Virology and Epidemiology of Viral Diseases, University Hospital Tübingen, Tübingen, Germany. [2]Institute for Molecular Virology and Cell Biology, Friedrich-Loeffler-Institut (FLI), Greifswald-Insel Riems, Germany. [3]Institute of Virology, Helmholtz Zentrum München, German Research Center for Environmental Health, Munich, Germany. [4]Bernhard Nocht Institute for Tropical Medicine, Hamburg, Germany. [5]German Center for Infection Research, Partner site Hamburg-Lübeck-Borstel-Riems, Hamburg, Germany. [6]Present address: Department of Infectious Diseases, Molecular Virology, Heidelberg University, Heidelberg, Germany. [7]These authors contributed equally: Dan Hu, Elena Hagelauer. ✉E-mail: michael.schindler@med.uni-tuebingen.de

© The Author(s)

mainly through macropinocytosis and transported to NPC intracellular cholesterol transporter 1 (NPC1)-positive endo-lysosomes, where GP is cleaved by cathepsin B/L and subsequently interacts with the main entry receptor NPC1 to induce virus-host membrane fusion and nucleocapsid release (Aleksandrowicz et al, 2011; Chandran et al, 2005; Côté et al, 2011; Saeed et al, 2010; Schornberg et al, 2006; Spence et al, 2016). The EBOV nucleocapsid contains the negative-stranded RNA genome, the RNA polymerase L, the nucleoprotein (NP), VP35, VP30, and VP24 (Bharat et al, 2012; Elliott et al, 1985; Huang et al, 2002; Hume and Mühlberger, 2019; Takamatsu et al, 2022). The viral genome comprises seven genes encoding seven structural proteins (NP, VP35, VP40, GP, VP30, VP24, and L) and two nonstructural proteins (sGP and ssGP) (Mehedi et al, 2011; Sanchez et al, 1993; Sanchez et al, 1996; Volchkov et al, 1995). EBOV genome replication and transcription take place in EBOV inclusion bodies (IBs) in the cytoplasm (Hoenen et al, 2012; Lier et al, 2017; Nanbo et al, 2013). IBs were recently characterized as liquid organelles, their formation is dependent on NP oligomerization and they recruit a number of viral as well as host proteins (Bodmer et al, 2023; Dolnik et al, 2021; Wu et al, 2023). Progeny virions are assembled and released from the plasma membrane, which is mainly driven by matrix protein VP40 and enhanced by NP and GP (Jasenosky et al, 2001; Licata et al, 2004).

Tetraspanins are a family of proteins that harbor four transmembrane helices, which are connected by three domains, a large and a small extracellular as well as one small intracellular domain (Charrin et al, 2014; Levy and Shoham, 2005). Tetraspanins are known to form tetraspanin-enriched microdomains with other host proteins, including integrins and actin linkers, and they are involved in multiple cellular processes, such as cell adhesion, migration, fusion, protein trafficking and signaling (Berditchevski and Odintsova, 2007; Maecker et al, 1997; Termini and Gillette, 2017; Yáñez-Mó et al, 2009). They are furthermore canonical components and marker proteins for extracellular vesicles, especially CD81, the related CD9 and CD63 (Andreu and Yanez-Mo, 2014). Tetraspanins also play multiple roles in the context of viral infections. CD81 is the main entry receptor of HCV and is downregulated upon infection to prevent superinfection of cells and activate pro-survival NFκB signaling (Bunz et al, 2024). In HIV-1 infection, CD81 might serve as an assembly hub (Jolly and Sattentau, 2007; Nydegger et al, 2006), is enriched in intracellular virus-containing compartments in macrophages (Deneka et al, 2007; Koppensteiner et al, 2012) and is downregulated by HIV-1 Vpu to increase viral particle infectivity (Lambele et al, 2015). Apart from these dual roles in viral infection, in which CD81 might act pro- or antiviral, dependent on the phase of viral replication, CD81 was also described as a host-dependency factor, facilitating replication of Chikungunya virus or Herpes simplex virus (Benayas et al, 2020; Lasswitz et al, 2022). However, not only CD81, but also other tetraspanins as for instance CD151, CD82, or CD63 play multiple roles during the replicative cycle of various viruses (Florin and Lang, 2018), which might not come as a surprise given the large functional diversity of tetraspanins in organizing membrane-related processes viruses have to cope with for viral entry, release as well as viral protein translation and maturation.

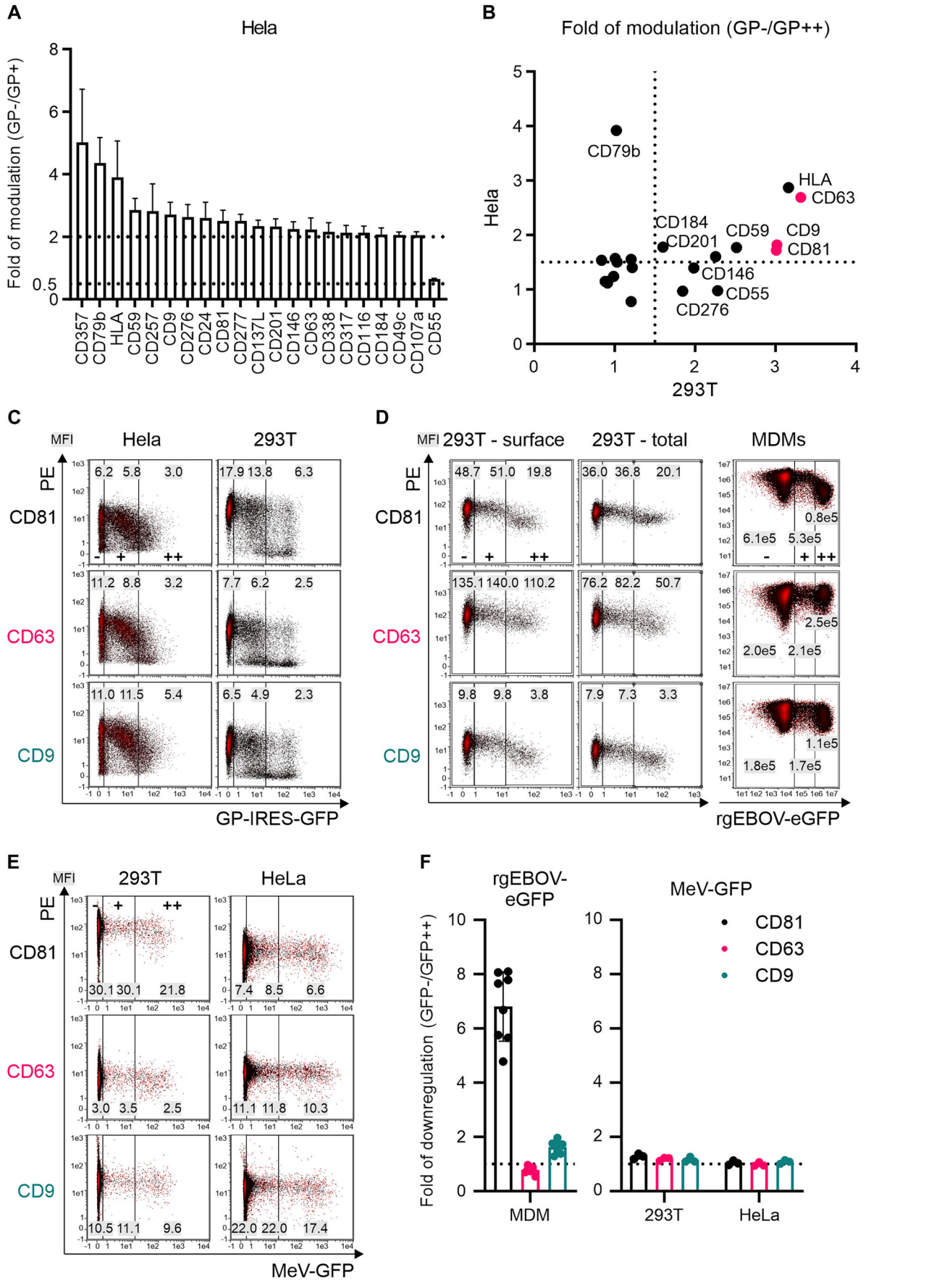
The viral surface glycoprotein EBOV GP is not only required for viral entry, but also known to modulate host proteins involved in viral pathogenesis and immune evasion (Francica et al, 2010; Kaletsky et al, 2009; Nehls et al, 2019; Simmons et al, 2002; Sullivan et al, 2005; Volchkov et al, 1998; Zampieri et al, 2007). To identify novel cell surface plasma membrane-residing proteins specifically modulated by EBOV GP, we performed a flow cytometry-based screen. Three tetraspanins, CD81, CD63, and CD9, were identified to be targeted by EBOV GP. We here analyzed the role of CD81, CD63, and CD9 in the EBOV life cycle and found CD81 to exert inhibitory activity on viral entry and EBOV replication.

Results

EBOV GP reduces cell surface expression levels of tetraspanins CD81, CD63 and CD9

To identify EBOV GP-modulated plasma membrane-residing proteins, a flow cytometry-based screen was performed. HeLa cells were transfected to express EBOV GP together with GFP via a bicistronic mRNA allowing to specifically identify cells that express GP (GFP-positive cells) and compare them to non-GP (GFP-negative) expressing cells in the same measurement (Fig. EV1). Importantly, high GP levels might induce cytotoxicity and cell death that could compromise our results. However, we did not detect altered forward or sideward scatter in our flow-cytometry plots upon GP-expression or increased Annexin V-staining, as a proxy for apoptosis (Fig. EV1). Next, cells were stained with PE-labeled antibodies against 332 plasma membrane proteins in a 96-well format and subjected to medium-throughput flow cytometry measurement. GP-mediated fold of surface protein downmodulation was calculated by dividing the MFI (mean fluorescence intensity) of the non-GP (GFP-negative) population by the MFI of the GP-expressing (GFP-positive) cells. EBOV GP modulated surface proteins were identified according to a threshold of modulation >2-fold (Dataset EV1), and 21 receptors (Fig. 1A) were selected for further validation in HeLa and 293T cells (Fig. 1B; Dataset EV2). HLA, CD81, CD63, CD9, CD201 (endothelial protein C receptor), CD184 (C-X-C chemokine receptor type 4), and CD59 showed reduced cell surface levels upon EBOV GP-expression in both cell lines (Figs. 1B and EV2A,B). HLA was reported before to have lower accessibility to antibodies due to shielding by EBOV GP glycans (Francica et al, 2010). Hence, reduced cell surface detection could be due to shielding of receptors or their removal and internalization, i.e., active downregulation. We next decided to focus on CD81, CD63, and CD9, since these three proteins belong to the tetraspanin family and were all affected by GP (Fig. 1A–C). Reduced cell surface levels of these three tetraspanins was confirmed in the context of authentic EBOV infection in which both surface and total cellular CD81, CD63, and CD9 were affected (Fig. 1D). Strikingly, lower levels of CD81 and to a lesser extent CD9 were also detected at the cell surface of primary human monocyte-derived macrophages (MDM) infected with authentic EBOV (Fig. 1D). In order to distinguish general viral effects from EBOV-specific mechanisms, measles-virus (MeV) infection was included as a control throughout this study. Like EBOV, MeV is an enveloped, negative-sense RNA virus, but it employs distinct entry and release mechanisms (Salditt et al, 2010). The tetraspanins were not modulated upon measles-virus (MeV)-infection (Fig. 1E,F). Taken together, EBOV GP modulates the tetraspanins CD81, CD63, and CD9 in 293T and HeLa cells as well

 © The Author(s)


A
Hela
Fold of modulation (GP-/GP+)
CD357 CD79b HLA CD59 CD257 CD9 CD276 CD24 CD81 CD277 CD137L CD201 CD146 CD63 CD338 CD317 CD116 CD184 CD49c CD107a CD55
B
Fold of modulation (GP-/GP++)
Hela
293T
CD79b
HLA
CD63
CD184
CD201
CD59
CD9
CD81
CD146
CD55
CD276
C
MFI
Hela
293T
PE
CD81
CD63
CD9
GP-IRES-GFP
D
MFI
293T - surface
293T - total
MDMs
rgEBOV-eGFP
E
MFI
293T
HeLa
MeV-GFP
F
rgEBOV-eGFP
MeV-GFP
Fold of downregulation (GFP-/GFP++)
CD81
CD63
CD9
MDM
293T
HeLa

© The Author(s)

Figure 1. EBOV GP downregulates tetraspanins CD81, CD63, and CD9.

(**A**) EBOV GP downmodulated surface receptors identified in HeLa cells with a flow cytometry-based screen (Dataset EV1). Shown are mean values of fold of modulation, calculated by dividing PE mean fluorescence intensity (MFI) of GP negative (GFP−) population by PE MFI of GP positive (GFP+) population, ±SD ($n = 3$). (**B**, **C**) Confirmation of EBOV GP-mediated modulation of the identified receptors in 293T and HeLa cells with flow cytometry (see also Fig. EV2; Dataset EV2). Shown are (**B**) mean values of fold of modulation ±SD ($n = 3$), and (**C**) representative density plots of cells expressing no (−), medium (+) to high (++) levels of GFP and hence GP (see also Fig. EV2A,B). (**D**, **F**) 293T cells and monocyte-derived macrophages (MDMs) were infected with authentic rgEBOV-eGFP (MOI = 1 and MOI = 0.5, respectively). 24 h.p.i. (293T) or 6 d.p.i. (MDMs), the cells were harvested and analyzed for surface and total expression of CD81, CD63 and CD9 by flow cytometry. Shown are (**D**) representative density plots and (**F**) mean values of fold of modulation (GFP−/GFP++) ±SD ($n = 8$ different donors from 2 independent experiments). (**E**, **F**) 293T and HeLa cells were infected with measles-virus (MeV-GFP, MOI = 0.1). 48 h.p.i., the cells were harvested and analyzed for surface expression of CD81, CD63,and CD9 by flow cytometry. Shown are (**E**) representative density plots and (**F**) mean values of fold of modulation (GFP−/GFP++) ±SD ($n = 3$). Values in the primary density plots indicate the PE MFI in the respective region. Source data are available online for this figure.

as in the context of authentic EBOV infection in primary macrophages.

Tetraspanin modulation is specific for filoviral GPs

To determine whether the tetraspanins are also affected by other filoviruses, 293T cells were transfected to express GP of Marburg virus (MARV), Sudan virus (SUDV), Reston virus (RESTV), and Taï Forest virus (TAFV). All filoviral GPs were able to reduce CD81, CD63, and CD9 surface levels, suggesting that tetraspanin modulation is a conserved feature of various members of the *Filoviridae* family (Fig. 2A). Next, we characterized GP1/2 domains (Fig. 2B) and several GP mutants (Fig. EV2C–E). Neither GP1 nor GP2 alone induced significant tetraspanin modulation (Fig. 2B). Notably, GP2 was not detectable by Western blot when expressed individually, and therefore, no conclusion can be drawn here regarding its potential to modulate tetraspanins (Fig. EV2D). The GP mutants tested had altered residues in the receptor-binding site (RBD, located in GP1), the fusion loop (FL, located in GP2), and the transmembrane domain (TM, located in GP2), all of which have been previously shown to be important for GP functionality (Fig. EV2C). All GP mutants still reduced CD81, CD63, and CD9 levels, although two mutations in the RBD (L111A and L122A), two mutants with altered residues in the FL (531A532A533A and 535A536A537A), and the ZLZ mutant (TM is changed to the TM of LASV GP) were less effective (Fig. EV2E). We further analyzed whether non-filoviral GPs might dysregulate CD81, CD63, or CD9. For this, a set of previously characterized viral GPs were transfected to be expressed in 293T cells together with GFP and assessed for cell surface tetraspanin levels (Fig. 2C). Of note, apart from EBOV GP, none of the tested GPs affected any of the three tetraspanins, suggesting that modulation of CD81, CD63, and CD9 is a specific feature of filoviral GPs.

CD81, but not CD63 and CD9, suppresses EBOV trVLP replication

To reveal why EBOV interferes with CD81, CD63 and CD9, the EBOV trVLP assay was used (Watt et al, 2014), as this system allows to analyze and model the different aspects of the EBOV life cycle under BSL2 conditions. 293T and Huh7.5 control, CD81 KO, CD63 KO, and CD9 KO cells were generated using CRISPR/Cas9 and KO confirmed by flow cytometry (Appendix Fig. S1A,B). 293T control and KO cells were transfected to express EBOV proteins of the ribonucleoprotein (RNP) complex (NP, L, VP35 and VP30), a tetracistronic (4cis) minigenome encoding a nanoluciferase (nluc) reporter as well as the remaining three EBOV proteins (GP, VP40, and VP24) and a plasmid expressing T7 RNA polymerase, mediating the initial transcription of the minigenome. Expression levels of the EBOV matrix protein VP40, encoded by the minigenome and therefore reflecting EBOV minigenome replication and transcription, were analyzed in both cell lysates and culture supernatants (medium) by Western blot. WT and a GP-deleted (dGP) minigenome were used to compare the effect of CD81, CD63, and CD9 on trVLP replication with and without GP expression.

KO of CD81, but not CD63 and CD9, led to significantly higher VP40 levels in cells and supernatants of trVLP-dGP producing cells. Similar results were observed in cells producing WT trVLP, suggesting a negative role of CD81 in EBOV trVLP viral RNA synthesis and/or protein expression (Fig. 3A). Besides, KO of CD81 resulted in higher increase in VP40 levels in cells (and supernatants) producing trVLP-dGP (~4,19) as compared to wildtype trVLP (~2,87), consistent with the possibility that EBOV GP might attenuate the inhibitory effect imposed by CD81 (Fig. 3A). Furthermore, VP40 levels in cell culture supernatants were normalized to VP40 in cell lysates, which revealed that KO of CD81 (as well as CD63 and CD9) had no measurable effect on trVLP release in this system (Fig. 3A). The aforementioned results were recapitulated and confirmed independently in Huh7.5 hepatocellular carcinoma cells (Fig. 3B) and employing a GFP-encoding trVLP construct, monitoring virus production over several days using GFP as a proxy (Appendix Fig. S1C). In both cell lines, albeit more pronounced in Huh7.5 cells, KO of CD81 increased GFP expression in the absence of GP (trVLP-dGP-GFP), likely due to the absence of CD81 antagonism (Appendix Fig. S1C). In general, VP40 and reporter gene expression was higher in trVLP-dGP producer cells than in trVLP-WT producer cells, which might be related to the inverse correlation between minigenome length and efficiency of viral protein expression (Appendix Fig. S1D and Watt et al, 2014). Altogether, the data indicate that CD81, but not CD63 and CD9, suppresses EBOV trVLP replication in 293T and Huh7.5 cells.

To confirm the suppressive role of CD81 in EBOV trVLP replication in another independent experimental setting, CD81 expression in 293T CD81 KO cells was restored by exogenously expressing increasing amounts of HA-tagged CD81 (CD81-HA). trVLP VP40 as well as nluc expression (reflecting viral RNA synthesis/gene expression) were analyzed by Western blot and luciferase activity assay. In accordance with our previous results, not only VP40 but also nluc expression increased upon KO of CD81 (Fig. 3C). Furthermore, expression of CD81 reduced VP40

 © The Author(s)

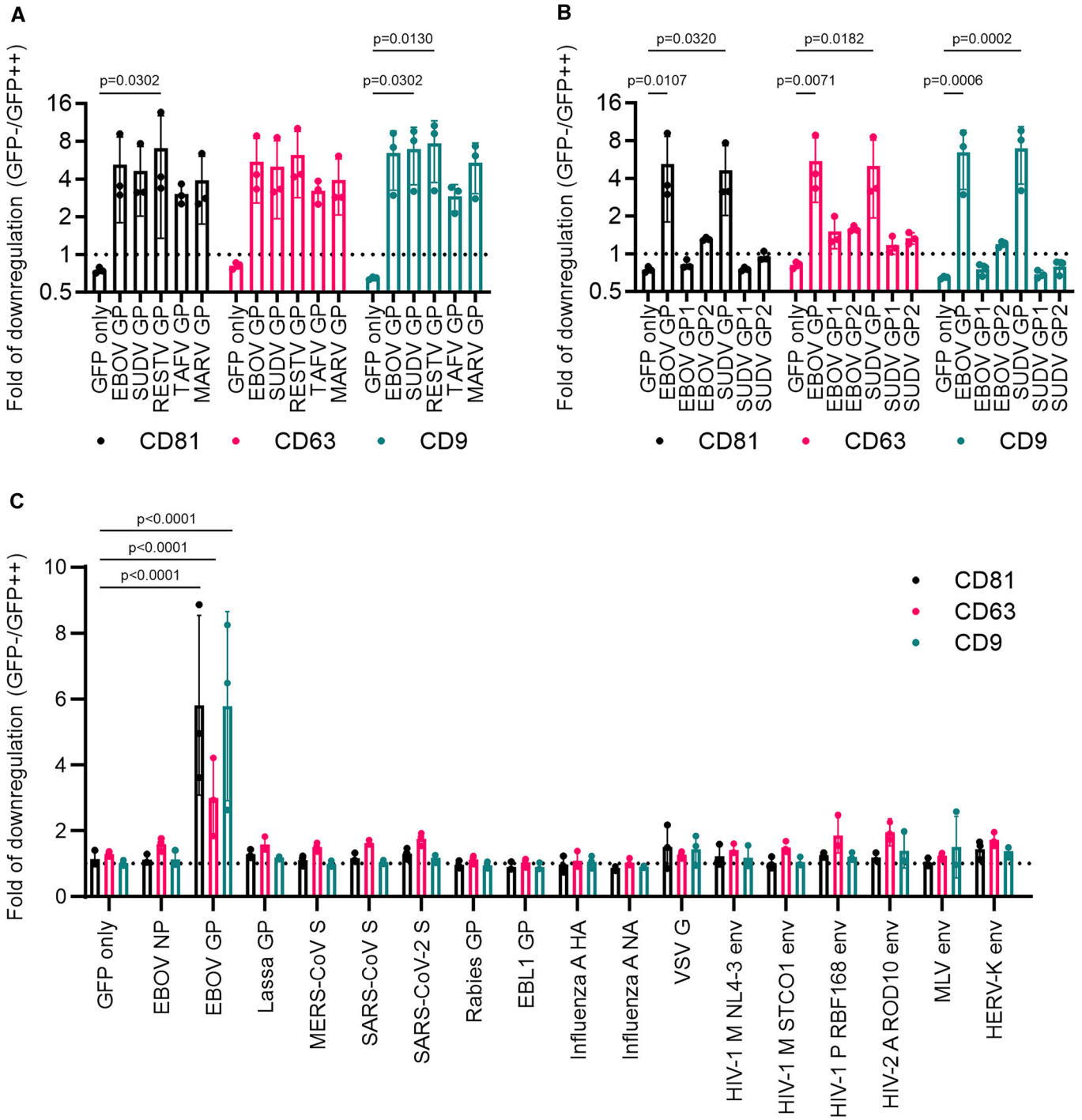
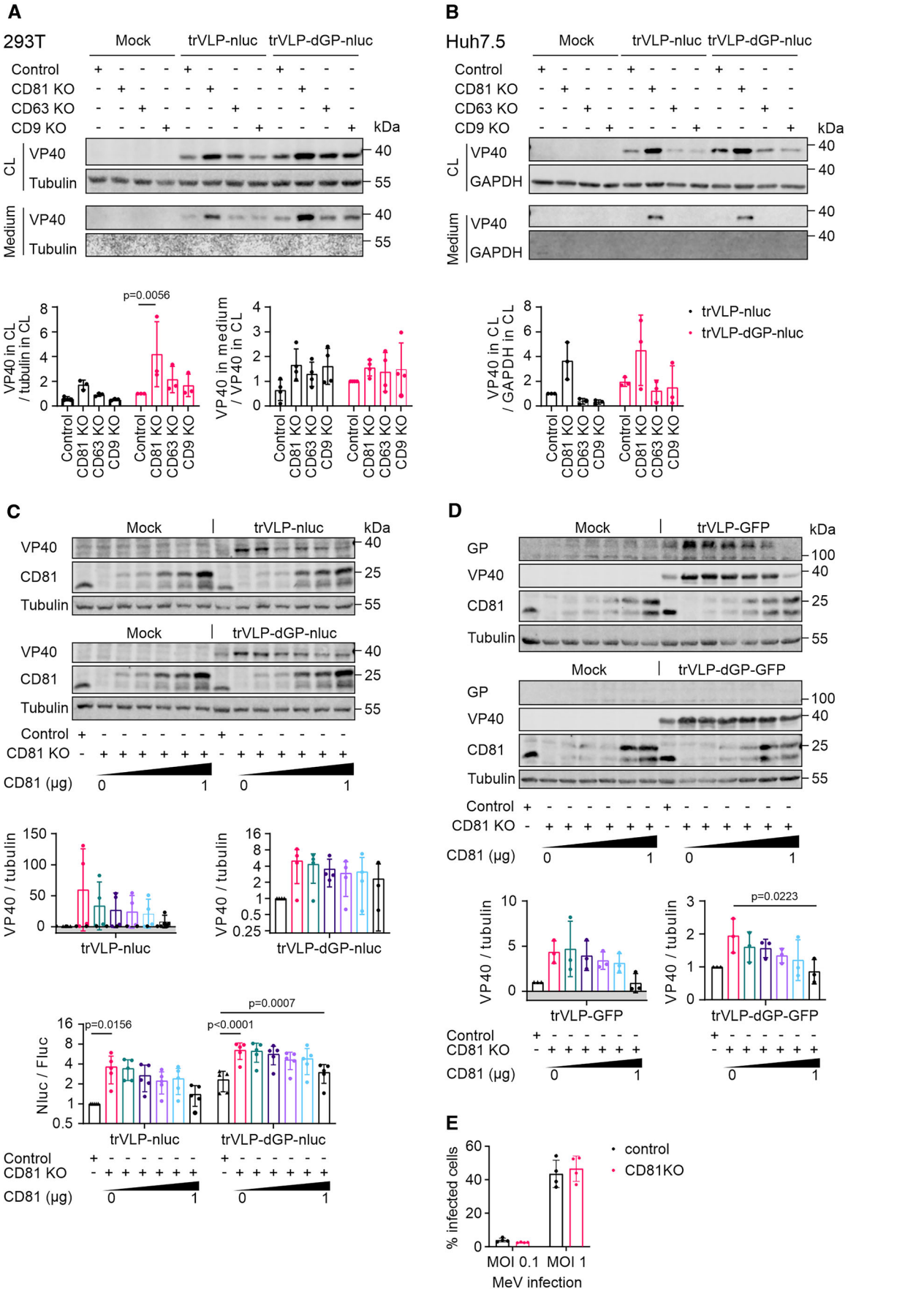


Figure 2. CD81, CD63, and CD9 downregulation is conserved among EBOV strains but not other viral glycoproteins.

(**A–C**) 293T cells were transfected to express GFP-only, or the (**A**) indicated filoviral GPs, (**B**) GP subunits, or (**C**) viral glycoproteins together with GFP. 2 d.p.t., the cells were harvested and analyzed for surface expression of CD81, CD63 and CD9 by flow cytometry. Indicated are mean values of fold of modulation (GFP−/GFP++) ±SD ($n = 3$). Two-way ANOVA with Dunnett correction was used for statistical analysis. Source data are available online for this figure.

and nluc expression in a dose dependent manner in 293T CD81 KO cells (Fig. 3C). To exclude the possibility that CD81 interferes with T7 polymerase mediated initial transcription of the 4cis-minigenome, a similar experiment was performed with an RNA polymerase II (pol II) driven 4cis-minigenome plasmid, which has similar gene organization as the T7 driven 4cis-minigenome. Similarly, KO of CD81 resulted in increased GP and VP40 expression, and exogenous expression of CD81 in CD81 KO cells reduced GP and VP40 expression (Fig. 3D). Finally, we again included MeV as a negative control, which showed, unlike EBOV

© The Author(s)


A
293T
Mock
trVLP-nluc
trVLP-dGP-nluc
Control
CD81 KO
CD63 KO
CD9 KO
kDa
CL
VP40
Tubulin
Medium
40
55
p=0.0056
VP40 in CL / tubulin in CL
VP40 in medium / VP40 in CL
B
Huh7.5
GAPDH
VP40 in CL / GAPDH in CL
trVLP-nluc
trVLP-dGP-nluc
C
CD81
CD81 (μg)
VP40 / tubulin
p=0.0156
p=0.0007
p<0.0001
Nluc / Fluc
D
trVLP-GFP
trVLP-dGP-GFP
GP
100
25
p=0.0223
E
% infected cells
control
CD81KO
MOI 0.1
MOI 1
MeV infection

© The Author(s)

Figure 3. CD81, but not CD63 and CD9, suppresses EBOV trVLP replication.

In order to assess EBOV replication and transcription, cells were transfected with RNP expression plasmids and a tetracistronic minigenome plasmid encoding nLuc or GFP and EBOV VP40, GP, and VP24 (trVLP) or a GP-deleted minigenome plasmid (trVLP-dGP). (**A**) 293T and (**B**) Huh7.5 control, CD81 KO, CD63 KO, and CD9 KO cells were transfected for trVLP-nluc/-dGP-nluc replication and production. 3 d.p.t., cells and medium were harvested for WB analysis. Indicated are representative WB images and mean values of WB signal quantification (normalized to control cells producing trVLPs, ±SD) from $n = 3$ independent experiments. (**C**) 293T control and CD81 KO cells were mock or pre-transfected to express gradient amounts of CD81-HA. One day later, the cells were transfected to produce trVLP-nluc/-dGP-nluc. A Fluc expression plasmid was co-transfected as a transfection control for normalization. 3 d.p.t., an aliquot of the cells was harvested to analyze Nluc and Fluc activity, and the remaining cells were harvested for WB analysis. Indicated are mean values of WB signal quantification (normalized to control cells, ±SD) and mean values of Nluc activity (normalized to Fluc and control cells producing trVLP-nluc, ±SD) from $n = 4$–5 independent experiments. (**D**) 293T cells mock or pre- transfected to express gradient amounts of CD81-HA were transfected for trVLP-GFP and trVLP-dGP-GFP replication. 3 d.p.t., the cells were harvested for WB analysis. Indicated are mean values of WB signal quantification ±SD from $n = 3$ independent experiments. (**E**) As a specificity control, 293T control and CD81 KO cells were infected with MeV-GFP. 2 d.p.i., infected (GFP+) cells were quantified by flow cytometry. Shown are mean infection rates ±SD from $n = 4$ independent experiments. Two-way ANOVA with Dunnett correction was used for statistical analysis. Source data are available online for this figure.

similar infection levels in CD81 KO, as compared to control cells (Fig. 3E).

Altogether, the cumulated data assessing replication of various trVLP minigenomes in different cell systems with CD81 overexpression as well as KO conditions support a restricting role of CD81 in the EBOV life cycle that might be attenuated by GP.

Mechanism of EBOV GP and VP40-mediated interference with CD81

Given that potent cellular restrictions to virus replication might be antagonized by more than one mechanism, we sought to determine whether EBOV employs, in addition to GP, other viral proteins to modulate CD81. 293T cells were transfected to express GFP-only or coexpress GFP and EBOV proteins. Cell surface as well as intracellular CD81 expression were analyzed by flow cytometry. Of note, CD81 was also downregulated by VP40, albeit less potently than GP, at both surface and intracellular levels in 293T cells (Figs. 4A and EV3A). Since only CD81, but not CD63 and CD9, restricts EBOV trVLP replication, the potential role of CD81 in the downregulation of CD63 and CD9 by EBOV GP was investigated. CD63 and CD9 were reduced by EBOV GP regardless of CD81 expression, in both 293T and Huh7.5 cells (Fig. EV3B,C). Next, we aimed to assess if the viral proteins induce internalization and possibly degradation of cell surface CD81, or if CD81 might be shielded from antibody binding via the GP glycans. For this, 293T cells expressing EBOV GP or VP40 were treated with the proteasome inhibitor MG132 or the lysosome degradation inhibitor bafilomycin A1 (BafA1). Cell surface as well as total CD81 expression were analyzed by flow cytometry. MG132 and BafA1 slightly blocked GP-mediated reduction of surface CD81 and attenuated VP40-mediated CD81 reduction (Fig. 4B, upper panel, see primary flow cytometry plots). Furthermore, MG132 and BafA1 partially restored total CD81 levels upon GP expression and had an inhibitory effect on the ability of VP40 to reduce total CD81 (Fig. 4B, lower panel).

To assess the importance of the GP glycan shield for this phenomenon, we employed the GPΔmuc mutant that is devoid of the mucin-like domain, which is heavily glycosylated (Peng et al, 2022). On top, we treated GP-expressing cells with PNGase F to remove N-glycans before staining with CD81 antibodies or HLA-A (MHCI) as a control (Iraqi et al, 2020; Reynard et al, 2009) (Fig. 4C). Unexpectedly, GPΔmuc reduced cell surface MHCI and CD81 slightly less efficient than WT GP. Nevertheless, N-glycan removal by PNGase F partially restored cell surface antibody binding to MHCI and CD81 in GP-expressing cells (Fig. 4C, left panel). Of note, and as expected, when using non-glycosylated VP40 and HIV-1 Vpu, another tetraspanin-modulating viral protein (Lambele et al, 2015), PNGase F treatment had no impact on the modulation of MHCI or CD81 (Fig. 4C, right panel). Furthermore, neither GP nor VP40 transcriptionally impaired CD81 mRNA levels (Fig. 4D). In conclusion, CD81 surface and total expression levels are reduced via the concerted action of EBOV GP and VP40 involving pathways of proteasomal and lysosomal degradation, as well as CD81 surface shielding by GP.

EBOV GP and VP40 interact with CD81

We next analyzed whether GP or VP40 interact with CD81. First using the Kusabira-green (KG) based BiFC assay (see Methods for details) to assess CD81 and GP interaction, both proteins were expressed as fusion proteins with the N- or C- part of KG (KGN or KGC), and reconstitution of KG fluorescence can be measured as a proxy of protein interaction. Upon transfection of 293T cells to express the KGN/KGC fusions of GP and CD81, a strong increase in the percentage of KG expressing cells (KG+) could be measured, suggesting that both proteins interact (Fig. 5A). To corroborate this result, we employed flow-cytometry-based FRET that indicates close proximity of potential interaction partners at a distance below 10 nm (Banning et al, 2010; Lim et al, 2022). We further expanded the analysis to GPs from other EBOV species and assessed FRET with the GP1 and GP2 subunits of EBOV (Kuhl et al, 2011). Importantly, GP2 fused to YFP is stably expressed (Kuhl et al, 2011). In line with the KG assay, all tested GPs exerted FRET with CD81, albeit with differential efficacy, and GP2 alone was sufficient to induce FRET (Fig. 5B). Similarly, VP40 and CD81 resulted in FRET, that was clearly distinguishable from background signals arising from transfecting the fluorophores alone or expressing VP40 together with markers of the TGN or clathrin endocytic route (Fig. 5C). Furthermore, proximity-ligation assay (PLA) revealed puncta indicative of close proximity between GP and CD81, as well as between VP40 and CD81, supporting an interaction of these proteins in HeLa cells (Fig. 5D,E). This is corroborated by areas of pronounced colocalization detected by immunofluorescence staining (Fig. 5F). Altogether, using various complementary methodology, the data supports a model in which GP directly interacts with CD81. VP40 also associates with CD81, even though seemingly less efficient as compared to GP.

© The Author(s)

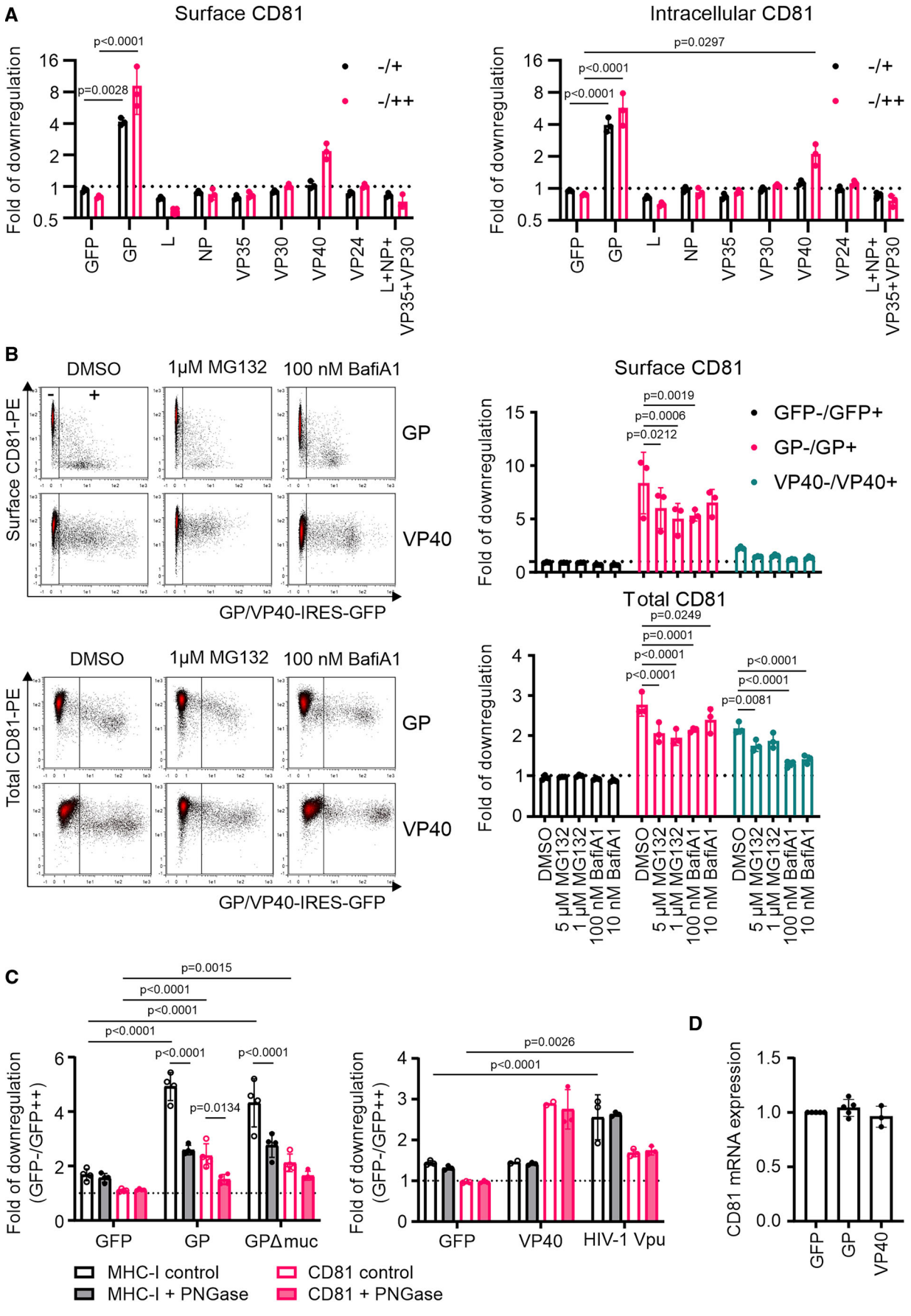

A
Surface CD81
Intracellular CD81
Fold of downregulation
-/+
-/++
p<0.0001
p=0.0028
p=0.0297
GFP
GP
L
NP
VP35
VP30
VP40
VP24
L+NP+ VP35+VP30
B
DMSO
1μM MG132
100 nM BafiA1
Surface CD81-PE
Total CD81-PE
GP
VP40
GP/VP40-IRES-GFP
GFP-/GFP+
GP-/GP+
VP40-/VP40+
p=0.0019
p=0.0006
p=0.0212
Total CD81
p=0.0249
p=0.0001
p=0.0081
DMSO
5 μM MG132
1 μM MG132
100 nM BafiA1
10 nM BafiA1
C
Fold of downregulation (GFP-/GFP++)
p=0.0015
p=0.0134
GPΔmuc
p=0.0026
HIV-1 Vpu
MHC-I control
MHC-I + PNGase
CD81 control
CD81 + PNGase
D
CD81 mRNA expression

Figure 4. Mechanism of EBOV GP and VP40-mediated downregulation of CD81.

(A) 293T cells were transfected to express GFP-only or coexpress GFP and EBOV proteins. 2 d.p.t., the cells were harvested for surface and intracellular CD81 staining and analyzed by flow cytometry. Indicated are mean values of the fold of modulation ± SD from $n = 3$ independent experiments. Plotted are fold modulations by dividing MFIs of cells that do not express the viral proteins (−) with MFIs of cells expressing medium (+) to high (++) levels of viral proteins according to GFP-expression (see also Fig. EV1). **(B)** 293T cells were transfected to express GFP-only or co-expressing GFP and GP or VP40. Six hours later, the cells were treated with DMSO only, MG132 or Bafilomycin A1. After 16 h incubation, the cells were harvested for surface (upper panel, non-permeabilized cells) and total (lower panel, permeabilized cells) CD81 staining and analyzed by flow cytometry. Indicated are mean values of the fold of modulation ± SD from $n = 3$ independent experiments and representative density plots. **(C)** 293T cells were transfected to express GFP-only, or GFP co-transfected with GP, a GP mutant that is lacking the mucin-like domain (GPΔmuc), VP40 or HIV-1 Vpu. 24 h.p.t. cells were left untreated or treated with PNGase (100 U/ml). Four hours later the cells were harvested and analyzed for CD81 surface expression. Shown are mean values of fold of modulation ± SD from $n = 4$ (left panel) or $n = 2$–3 (right panel) independent experiments. **(D)** CD81 mRNA levels of GP or VP40-expressing 293T cells were quantified by RT-qPCR. Data were normalized to GAPDH and presented as normalized to GFP-expressing cells. Shown are mean values ± SD from $n = 3$ (VP40) or $n = 5$ (GFP/GP) independent experiments. **(A–D)** Two-way ANOVA with Dunnett correction was used for statistical analysis. Source data are available online for this figure.

CD81 reduces overall levels of EBOV RNA species and suppresses VP40-induced NFκB activation

To elaborate which steps of EBOV trVLP replication are suppressed by CD81, we determined the effect of CD81 on EBOV trVLP mRNA, vRNA and cRNA synthesis in trVLP producer cells (Martínez et al, 2008; Mühlberger et al, 1999; Weik et al, 2002). Therefore, we measured RNA species in trVLP producer cells and found that KO of CD81 increased VP40 cRNA, and that there was also a trend to higher mRNA and vRNA levels (Fig. 6A). cRNA and vRNA levels are dependent on viral genome replication, whereas mRNA levels are dependent on both mRNA transcription and the amount of vRNAs available as template for this process, and thus on both replication and transcription. This indicates that CD81 interferes with minigenome replication (as seen by the reduction of cRNA levels), whereas it remains unclear whether there is also a CD81-mediated suppression of transcription.

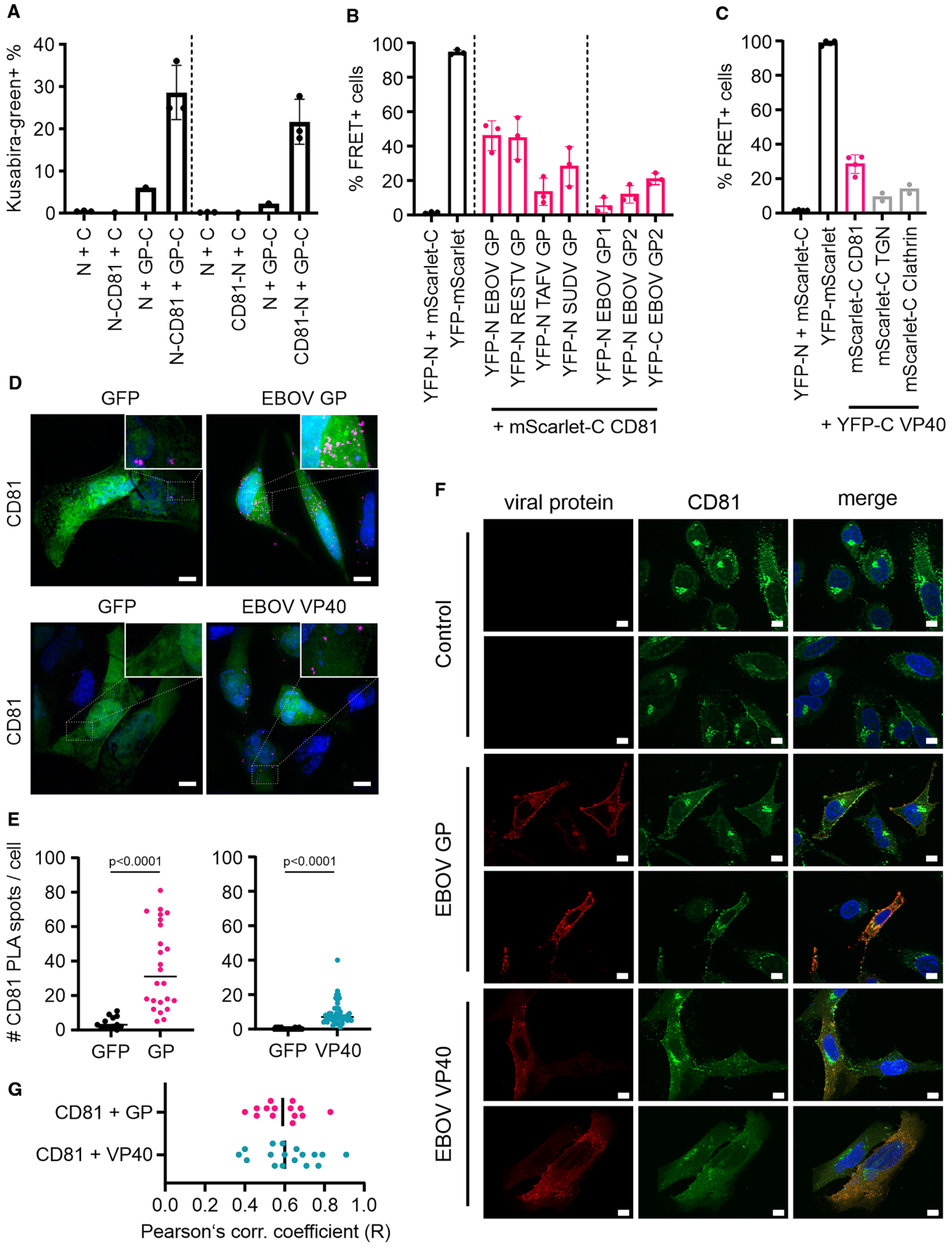
EBOV genome replication and transcription take place in EBOV IBs; a process requiring specific viral protein interactions (Hoenen et al, 2012; Lier et al, 2017). In this aspect, we sought to determine whether CD81 modulates EBOV IB formation. As previously described, the sole expression of NP allows the formation of a dot-like structure of IBs, and VP35 interacting with NP contributes to IB formation and viral RNA synthesis (Groseth et al, 2009; Miyake et al, 2020). Additionally, VP35 is a chaperone of NP, regulating NP homo-oligomerization and NP-RNA binding (Kirchdoerfer et al, 2015; Leung et al, 2015). To investigate whether CD81 affects NP homo-oligomerization and NP-VP35 interaction, we again used the Kusabira-green-based BiFC assay. EBOV NP and VP35 were expressed as fusion proteins with either KGN or KGC, and reconstruction of KG represents protein oligomerization or interaction. KO of CD81 did not result in an increased number of cells showing NP, VP35 or NP to VP35 interaction (KG+ %) (Fig. EV4A). This indicates that CD81 does not have an impact on IB formation, which we independently confirmed by quantifying IB formation via immunofluorescence staining in cells expressing the RNP proteins, or in RNP-expressing cells infected with trVLPs (Fig. EV4B,C).

We recently demonstrated that CD81 can suppress NFκB activation (Bunz et al, 2024) and therefore hypothesized that NFκB is dysregulated by viral proteins in trVLP-infected cells, possibly in a CD81-dependent manner. To test for this, we first transfected 293T cells to express various EBOV proteins and analyzed NFκB-dependent luciferase reporter activity. Of note, VP40 expression resulted in a strongly increased luciferase signal as a proxy for NFκB activation, and this effect was even more pronounced in CD81 KO cells (Fig. 6B). We could also detect higher MFIs of endogenous p65 in VP40-expressing cells (Fig. 6C), a phenotype we corroborated in the context of trVLP infection (Appendix Fig. S2) and quantitative image analyses (Fig. 6D), supporting our observation of NFκB activation. Based on our previous data (Bunz et al, 2024), we hypothesized that CD81 might inhibit NFκB activation imposed by EBOV VP40. To test for this, we activated NFκB by transfection of VP40 and co-transfected 293T to express increasing amounts of CD81 (Fig. 6E). Of note, exogenous gradual CD81-expression reduced VP40-mediated NFκB signaling. This effect was specific for VP40-mediated NFκB activation, whereas CD81 did not suppress induction of NFκB triggered through constitutively active IKKβ (Fig. 6E). Altogether, EBOV VP40 activates NFκB signaling in 293T cells, in a way that is negatively regulated by CD81.

CD81 restricts early steps of EBOV trVLP infection

For some viruses, i.e., HCV and HPV, tetraspanins play important roles during viral entry and early infection (Bartosch et al, 2003; Gräßel et al, 2016; Mikuličić et al, 2020; Scheffer et al, 2013). To explore whether CD81, CD63 or CD9 are involved in early steps of EBOV infection, including entry, EBOV trVLP-GFP infection in 293T control, CD81 KO, CD63 KO, and CD9 KO cells was analyzed. In trVLP infection, the minigenome is replicated and transcribed only by pre-transfected EBOV RNPs and no T7/pol II-mediated initial transcription is involved. Of note, KO of CD81, but not of CD63 and CD9, resulted in increased GP and VP40 expression in trVLP-infected cells (Fig. 7A, left and quantification below). Similarly, KO of CD81 led to increased trVLP-GFP infection rates (Fig. 7A, right). An increased infection rate could result from more efficient entry and/or from altered minigenome replication/transcription, which we already demonstrated to be restricted by CD81 (Figs. 3 and 6). To specifically assess EBOV GP-mediated entry, 293T control, CD81 KO, CD63 KO, and CD9 KO cells were infected with GFP-expressing lentiviruses (lenti-GFP) pseudotyped with either EBOV GP or VSV G. The infection rates were analyzed by flow cytometry. KO of CD81, but not of CD63 and CD9, enhanced EBOV GP-, but not VSV G-mediated entry of lenti-GFP (Fig. 7B), suggesting a suppressive role of CD81 in EBOV GP-mediated entry. Vice versa, we employed trVLP-dGP-GFP pseudotyped with EBOV GP or VSV G for infection, revealing that CD81 KO enhanced the infection of trVLP-dGP-GFP irrespective of the GP used (Fig. 7C). Authentic EBOV or EBOV VLPs are

© The Author(s)


A
Kusabira-green+ %
40
30
20
10
0
N + C
N-CD81 + C
N + GP-C
N-CD81 + GP-C
N + C
CD81-N + C
N + GP-C
CD81-N + GP-C
B
% FRET+ cells
100
80
60
40
20
0
YFP-N + mScarlet-C
YFP-mScarlet
YFP-N EBOV GP
YFP-N RESTV GP
YFP-N TAFV GP
YFP-N SUDV GP
YFP-N EBOV GP1
YFP-N EBOV GP2
YFP-C EBOV GP2
+ mScarlet-C CD81
C
% FRET+ cells
100
80
60
40
20
0
YFP-N + mScarlet-C
YFP-mScarlet
mScarlet-C CD81
mScarlet-C TGN
mScarlet-C Clathrin
+ YFP-C VP40
D
GFP
EBOV GP
CD81
GFP
EBOV VP40
CD81
E
CD81 PLA spots / cell
100
80
60
40
20
0
p<0.0001
GFP
GP
p<0.0001
GFP
VP40
F
viral protein
CD81
merge
Control
EBOV GP
EBOV VP40
G
CD81 + GP
CD81 + VP40
0.0 0.2 0.4 0.6 0.8 1.0
Pearson's corr. coefficient (R)

© The Author(s)

Figure 5. EBOV GP and VP40 interact with CD81.

(**A**) 293T cells were transfected to express the N- and C- terminal fragment of Kusabira-green as a fusion protein with GP or CD81 as indicated and analyzed by flow cytometry. Mean values ± SD are shown from $n = 3$ independent experiments. (**B**) Filoviral GPs fused to YFP were co-transfected with a mScarlet-CD81 fusion protein in 293T cells. 24 h.p.t., cells were harvested and the FRET signal was measured by flow cytometry. Indicated are mean values ± SD from $n = 3$ independent experiments. (**C**) YFP was fused to the N-terminus of EBOV VP40 and co-transfected into 293T cells with mScarlet-CD81 or control mScarlet-fusion proteins localizing to the trans-Golgi network or clathrin-positive structures. 24 h.p.t., cells were harvested and FRET signal was measured by flow cytometry. Indicated are mean values ± SD from $n = 4$ (negative control, positive control, and VP40) or $n = 2$ (control mScarlet proteins) independent experiments. (**D**) HeLa cells were transfected to express GFP-only or EBOV GP or VP40 together with GFP from a bicistronic mRNA. 24 h.p.t. cells were stained for PLA using CD81- and GP- or VP40-specific antibodies, as detailed in the Methods section. (**E**) PLA dots per cell from two independent experiments were analyzed for statistical assessment (GFP controls $n = 13$ and $n = 21$, GP $n = 24$; VP40 $n = 48$). Median values are shown. Statistical significance was determined using a two-tailed non-parametric Mann–Whitney test. (**F**) HeLa cells, mock-transfected or transfected to express EBOV GP or VP40, were fixed 24 h.p.t. and stained for CD81 and GP or VP40. Shown are representative images of three independent experiments. Scale bars indicate a distance of 10 µm. (**G**) Colocalization was assessed in ImageJ using Pearson's correlation coefficient (R) in transfected cells from $n = 3$ independent experiments. Data are shown as individual transfected cells with the median indicated (CD81/VP40 $n = 17$, CD81/GP $n = 14$). Source data are available online for this figure.

internalized mainly through macropinocytosis (Aleksandrowicz et al, 2011; Nanbo et al, 2010; Saeed et al, 2010). We therefore studied whether CD81 has an effect on macropinocytosis by analyzing the uptake of Dextran-555, a fluid-phase marker, by flow cytometry. KO of CD81 enhanced the uptake of Dextran-555 in 293T cells (Fig. 7D), suggesting a role of CD81 in macropinocytosis. Dextran-555 uptake in Huh7.5 cells was less dependent on CD81 (Fig. EV5A) whereas in primary monocyte-derived macrophages (MDM) Dextran-555 internalization was clearly boosted upon CD81 KO (Fig. EV5B). In addition, we analyzed if infection of 293T cells with EBOV GP pseudotyped trVLPs is reduced by CD81 overexpression (Fig. EV5C) and found that high CD81 levels suppress trVLP infection in 293T cells (Fig. 7E). This confirms the negative role of CD81 in EBOV trVLP infection in 293T cells. Altogether, the cumulated data indicate that CD81 restricts EBOV trVLP cellular uptake and entry.

A CD81-crosslinking antibody inhibits EBOV infection

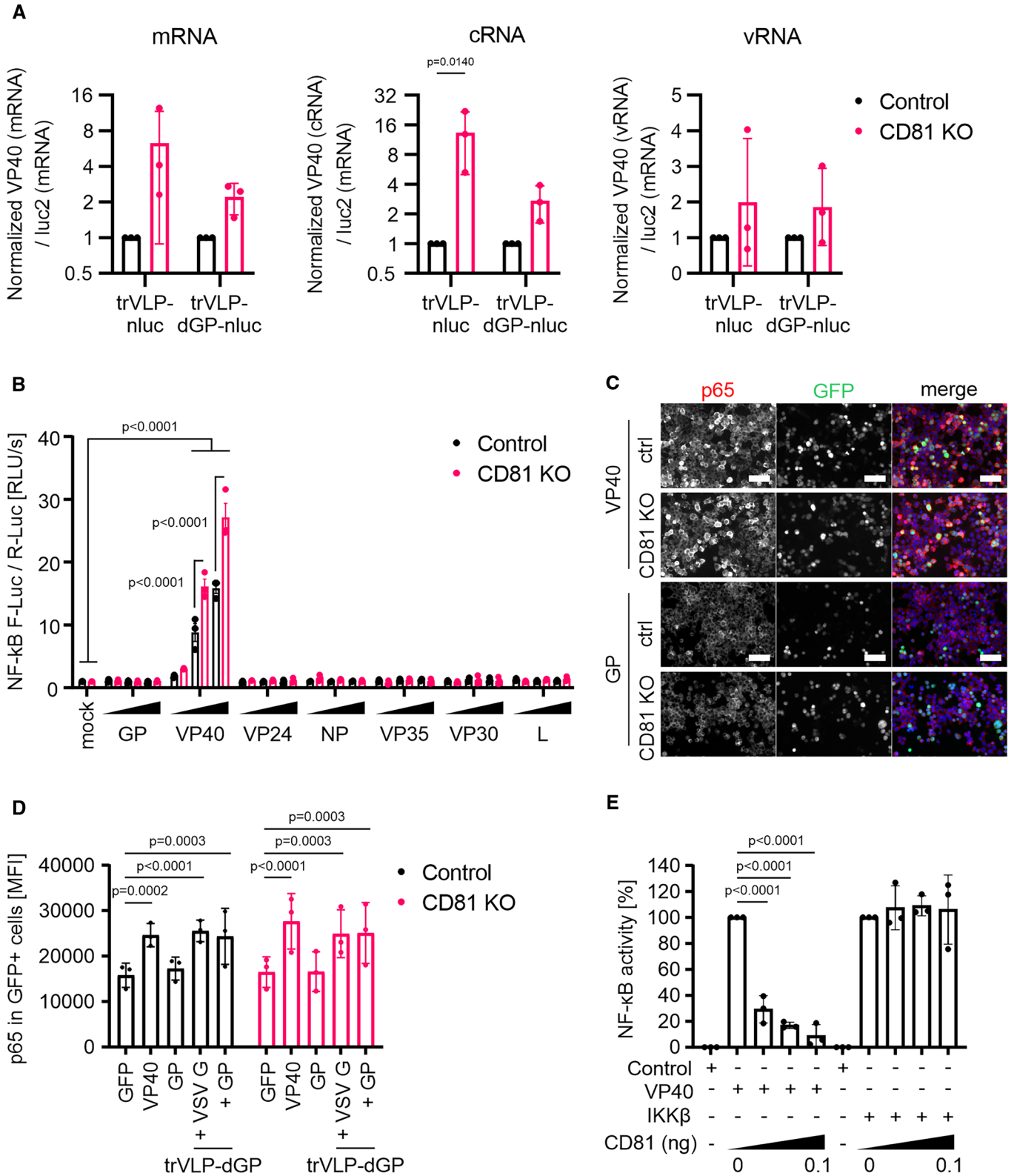
Since CD81 itself restricts EBOV trVLP infection at early and late steps of viral replication, we hypothesized that targeting CD81 with a crosslinking antibody that induces cell signaling could exert antiviral effects. The antibody 5A6 was initially identified to bind to CD81 and induce antiproliferative effects (Oren et al, 1990). 5A6 was further shown to bind to the large extracellular loop of CD81 and induce conformational changes and CD81 clustering at the cell surface (Susa et al, 2020; Vences-Catalán et al, 2021). Another study stated that 5A6 activates a caspase 3-PARP-triggered pathway (Vences-Catalán et al, 2019). Strikingly, CD81 5A6 pre-treatment at 1 or 5 µg/ml suppressed EBOV trVLP infection of CD81-expressing 293T cells when VLPs were pseudotyped with either GP or VSV G (Fig. 8A–C). Importantly, the effect is CD81 specific, since an isotype control antibody did not exert any antiviral effects, and the CD81 antibody did not reduce EBOV trVLP infection in CD81 KO cells. Even though, as expected, infection levels were generally higher in CD81 KO cells (Fig. 8B,C). Furthermore, moving to authentic infection systems, EBOV infection of 293T cells was also suppressed by CD81 antibody 5A6 treatment (Fig. 8D,E). In contrast, neither the CD81 antibody, nor the CD81 KO had any suppressive effect on MeV infection (Fig. 8F). Altogether, CD81 interferes with EBOV trVLP infection throughout the viral life cycle, affecting entry and replication. Targeting CD81 via the cell signaling-inducing antibody 5A6 specifically inhibits trVLP as well as authentic EBOV infection.

Discussion

By comprehensive assessment of cell surface protein levels in EBOV GP-expressing cells, we identified tetraspanins CD81, CD63, and CD9 to be dysregulated by EBOV GP. Not only EBOV GP but also MARV, SUDV, TAFV, and RESTV GP were able to interfere with surface CD81, CD63, and CD9. This effect was not observed with glycoproteins from other virus families tested, suggesting a conserved function among filovirus GP. Of note, GP seems to exert specificity in lowering levels of cell surface receptors, as of 332 receptors assessed by flow cytometry, 46 showed more than twofold reduced antibody binding and three receptors were increased upon GP expression (Fig. 1A; Dataset EV1). This is remarkable, as it was hypothesized that EBOV GP might form a glycan shield at the PM, that generally interferes with antibody binding and for instance lowers the accessibility of HLA towards cytotoxic T lymphocytes (CTL) (Francica et al, 2010; Simmons et al, 2002). Our study indicates that EBOV GP alters the composition of the PM by additional mechanisms. As exemplified for CD81, such mechanisms include, in addition to glycan shielding, direct or indirect protein interaction and therefore potentially interference with receptor localization, recycling and trafficking. The latter could involve GP-mediated alteration of protein turnover via the proteasomal and lysosomal routes. CD81 is not only modulated by GP, but also by VP40, indicating that EBOV exploits various independent mechanisms to antagonize and inactivate host cell suppression. It will be interesting to clarify the exact mechanistic interplay of these modalities in the process of GP and VP40-mediated alteration of CD81.

CD81 and CD9 share around 60% sequence similarity, and both tetraspanins have similar structures, while the extracellular loop sequence differs from each other (Umeda et al, 2020; Zimmerman et al, 2016). Therefore, since both CD81 and CD9 are down-regulated by GP, even though only CD81 is strongly modulated in primary macrophages (Fig. 1D,F), it is tempting to hypothesize that the shared intracellular sequence motif (Reppert and Lang, 2022) and transmembrane domain are involved in receptor modulation, while the unique sequence identity in CD81 (mainly located to the extracellular loops) confers the inhibitory role of CD81 on EBOV trVLP replication. In GP, mutations in the RBD, FP and TMD impaired CD81-modulation (Fig. EV2E). Hence, multiple sequence motifs in GP seem to participate in the complex interaction with CD81, that conceivably will involve domains necessary for functional interaction (for instance GP2), while others might direct CD81 for proteasomal and lysosomal degradation and contribute to

© The Author(s)


A
mRNA
cRNA
vRNA
Normalized VP40 (mRNA) / luc2 (mRNA)
Normalized VP40 (cRNA) / luc2 (mRNA)
Normalized VP40 (vRNA) / luc2 (mRNA)
p=0.0140
trVLP-nluc
trVLP-dGP-nluc
Control
CD81 KO
B
NF-κB F-Luc / R-Luc [RLU/s]
p<0.0001
mock
GP
VP40
VP24
NP
VP35
VP30
L
C
p65
GFP
merge
VP40
GP
ctrl
CD81 KO
D
p65 in GFP+ cells [MFI]
p=0.0003
p<0.0001
p=0.0002
GFP
VP40
GP
+ VSG + GP
trVLP-dGP
E
NF-κB activity [%]
Control
VP40
IKKβ
CD81 (ng)

 © The Author(s)

Figure 6. CD81 reduces levels of EBOV RNA species and suppresses VP40-induced NFκB activation.

(A) 293T control and CD81 KO cells were transfected for trVLP replication and transcription. 3 d.p.t., the cells were harvested for RNA extraction. vRNA, cRNA, and mRNA levels of VP40 and the luc2 (fluc) mRNA level were determined by RT-qPCR. Indicated are mean values (normalized to luc2 and further the control cells) ± SD from $n = 3$ independent experiments. **(B)** 293T control and CD81 KO cells were transfected to express increasing amounts of EBOV proteins, a reporter expressing Firefly-luciferase (F-Luc) under control of an NFκB responsive promoter and Renilla-luciferase for normalization (R-Luc). 24 h.p.t cells were harvested, lysed and subjected to luciferase measurement. Indicated are mean F-Luc values (normalized to R-Luc) ± SD from $n = 3$ independent experiments. **(C)** Similar setup as in **(B)**, however, 293T cells were analyzed by fluorescence microscopy and endogenous p65 was stained by IF, nuclei with DAPI and EBOV protein-expressing plasmids coexpress GFP via an IRES. Scale bars indicate a distance of 100 µm. **(D)** Quantification of p65 mean fluorescence intensity in GFP-positive 293T cells expressing the indicated EBOV proteins or previously infected with VSV G- or GP- pseudotyped EBOV trVLPs (Appendix Fig. S2). Indicated are mean values ± SD from $n = 3$ independent experiments. **(E)** 293T cells were transfected to express VP40 or a constitutively active mutant of IKKβ and an F-Luc NFκB reporter. Furthermore, a control vector or increasing concentrations of a CD81-expressing vector were transfected. Luciferase reporter activity was measured 24 h.p.t. Indicated are mean values, background subtracted and normalized to corresponding 0 ng CD81 condition ± SD from $n = 3$ independent experiments. **(A)** Two-way ANOVA with Šidák multiple comparison was used for statistical analysis. **(B, D, E)** Two-way ANOVA with Dunnett's multiple comparison was used for statistical analysis. Source data are available online for this figure.

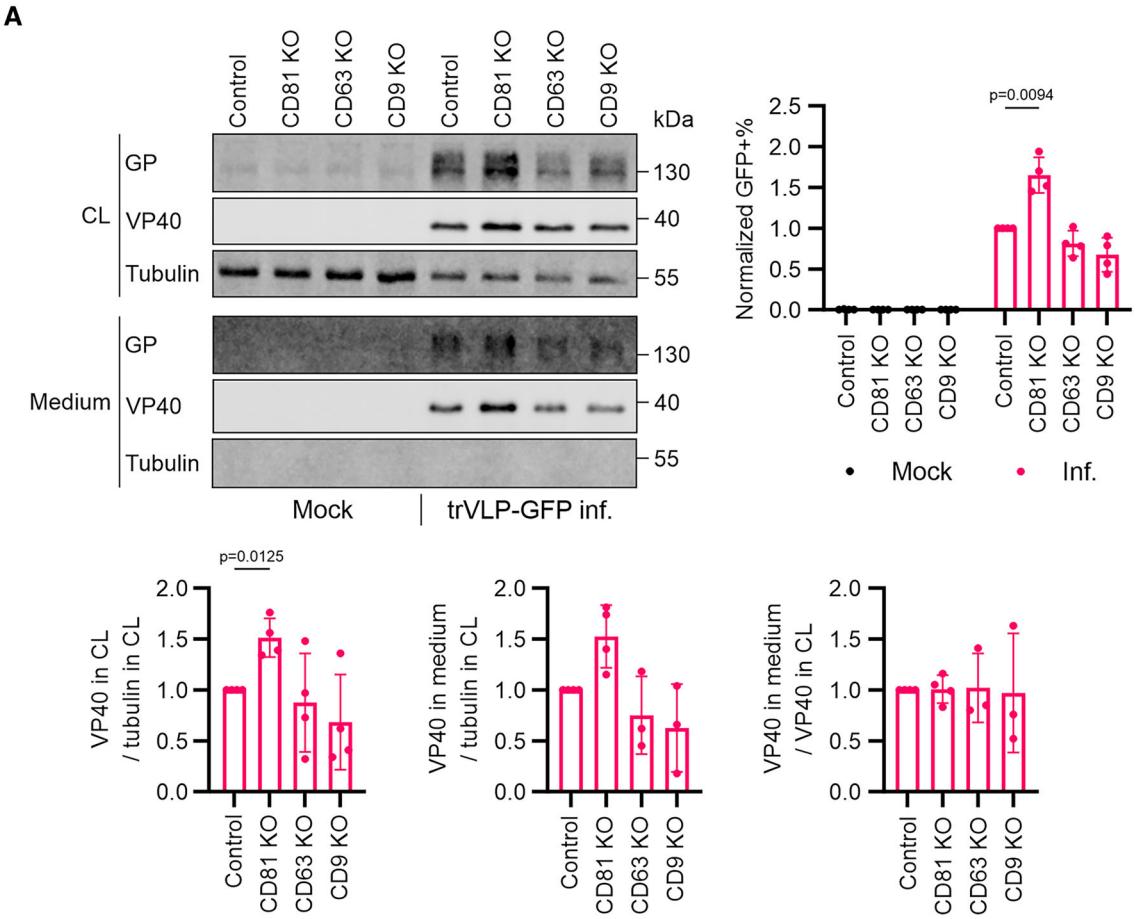
glycan shielding (GP1). Such a scenario is also supported by modeling GP together with CD81, suggesting protein interactions mainly via the transmembrane spanning alpha helices of both proteins, but also via proximal regions (Appendix Fig. S3). Consequently, extensive and systematic mutagenesis of GP, VP40, and CD81 to identify structural motifs and minimal regions that mediate different aspects and functional consequences of CD81-modulation is needed.

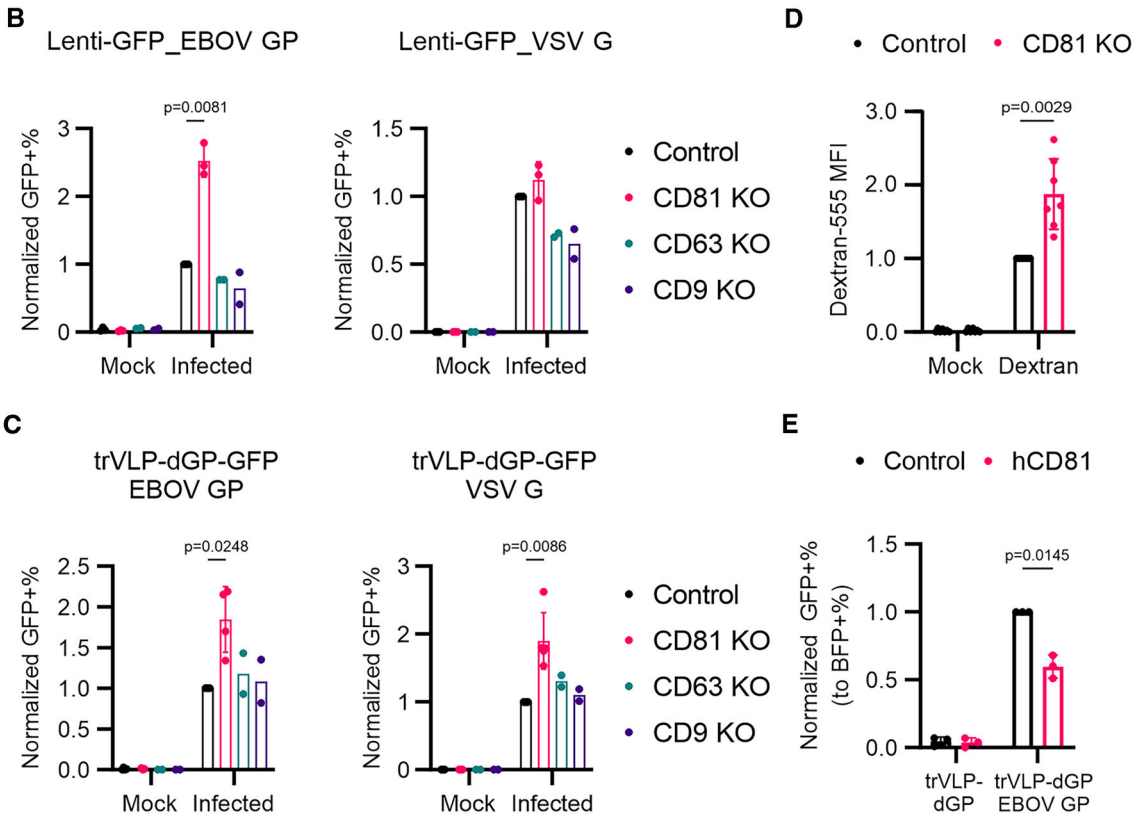
Our studies firmly establish CD81, but not CD63 or CD9, as an inhibitory factor acting at the level of entry and replication within the EBOV life cycle. Importantly, our findings are not at odds with a recent report suggesting a beneficial role of CD9 in acting as a cofactor in VP40 VLP release (Anand et al, 2026). However, as CD9 KO did not result in a pronounced phenotype in 293T or Huh7.5 cells (Fig. 3A,B), we focused on CD81. CD81 suppresses levels of EBOV RNA species, mainly the cRNA, while IB formation that is essential for efficient EBOV genome replication and transcription, seems not affected by CD81 (Groseth et al, 2009; Hoenen et al, 2012; Lier et al, 2017; Mühlberger et al, 1999; Nanbo et al, 2013). Another restriction imposed by CD81 includes GP-dependent and independent routes of entry, involving a not-yet discovered role of CD81 in macropinocytosis. It is remarkable that upon employing lentiviruses pseudotyped with either GP or VSV G, only GP-driven entry was restricted by CD81, indicating a direct inhibitory effect of CD81 on GP (Fig. 7B). In contrast, trVLPs pseudotyped with GP or VSV G exerted CD81-dependency (Fig. 7C). This suggests the filoviral envelope as another determinant of CD81-dependent entry, possibly through interaction of phosphatidyl-serines (PtdSer) with PtdSer-receptors, that are internalized during macropinocytosis in a CD81-dependent manner. The herein reported functional role of CD81 in macropinocytosis is in line with CD81 regulation of the GTPase Rac and its importance for macropinocytosis (Fujii et al, 2013; Tejera et al, 2013). Besides, CD81 is also related to ERMs (Ezrin-Radixin-Moesin), actin-binding proteins that are also involved in macropinocytosis (Chiasson-MacKenzie et al, 2018; Sala-Valdés et al, 2006) and to PI3K-AKT signaling (Martins et al, 2019), another central mediator of macropinocytosis (Kay, 2021). The direct role of CD81 in GP-mediated attachment and entry could be related to the CD81-interaction partners integrin α1, 4, 5, 6 and β1 (Domanico et al, 1997; Oguri et al, 2020; Serru et al, 1999). Integrin α5β1 is involved in EBOV entry by regulating cathepsins (Schornberg et al, 2009; Simmons et al, 2002; Zampieri et al, 2007). Our flow cytometry screen includes antibodies against integrins, αβ1, β5, and β7 (Dataset EV1). However, none of them is modulated by GP. Extending our analysis to other CD81 interaction partners that are non-TSPs and assessed by our approach, neither CD19 (Horvath et al, 1998) nor CD44 (Ramos et al, 2022) are GP-modulated (Dataset EV1). This, and the fact that GP directly interacts with CD81 (Fig. 5), argues against a mechanism in which CD81-interference is a bystander effect of GP modulating another CD81-interaction partner. In the future, it will be highly interesting to dissect these different EBOV entry-related effects of CD81 and the functional consequences arising, including the possibility to modulate superinfection and viral spread.

Of note, the inhibitory effects of CD81 on EBOV replication could be related to its ability to suppress NFκB signaling (Bunz et al, 2024). NFκB is a pleiotropic transcription factor that has profound effects on cellular proliferation, apoptosis and organization of the cytoskeleton and is also affected by the endocytic machinery (Banan et al, 2004; Maminska et al, 2016; Nemeth et al, 2004; Oeckinghaus and Ghosh, 2009). On top, it is an important factor boosting the interferon antiviral response (Sharma et al, 2003). In this regard, given that EBOV efficiently blunts the innate immune response (Basler et al, 2003; Cardenas et al, 2006; Chang et al, 2009; Harcourt et al, 1999), the sustained NFκB activation in the absence of innate immune signaling likely results in an overall proviral and replication-supportive cellular environment (Luo et al, 2005; Verzella et al, 2020). 293T cells employed here neither express tetherin (also known as BST2) nor TLR4, that were previously implied to activate NFκB in cooperation with GP and VP40 (Okumura et al, 2010; Rizk et al, 2017). We hence demonstrate that VP40 activates NFκB, and this phenotype is confirmed in EBOV trVLP-infected cells. Most importantly, this finding is supported by a recent study that extended this phenotype to VP40 proteins of other filoviruses and suggested a mechanism that is triggered via the TNFR1 signaling axis (Yamaoka et al, 2026). Given the importance of NFκB activation during EBOV infection in driving the cytokine storm and immunopathogenesis (Basler, 2017; Scherm et al, 2022), our and Yamaoka et al findings reveal a previously unrecognized, TLR4-independent mechanism of NFκB activation by EBOV VP40.

Finally, it is striking that the cell signaling-inducing CD81 antibody 5A6, targeting the extracellular loop of CD81, suppressed infection of 293T cells with EBOV trVLPs pseudotyped with GP or VSV G, as well as authentic EBOV infection (Fig. 8). In contrast, pre-treatment with the 5A6 antibody had no effect on MeV replication, indicating a filovirus-specific activity. 5A6 has been shown to inhibit breast cancer cell invasion and migration, and B cell lymphoma growth with good safety profiles in mice via activation of cell signaling (Vences-Catalán et al, 2019; Vences-

© The Author(s)


A
Control
CD81 KO
CD63 KO
CD9 KO
kDa
CL
GP
VP40
Tubulin
Medium
130
40
55
Mock
trVLP-GFP inf.
Normalized GFP+%
p=0.0094
Mock
Inf.
p=0.0125
VP40 in CL / tubulin in CL
VP40 in medium / tubulin in CL
VP40 in medium / VP40 in CL


B
Lenti-GFP_EBOV GP
Lenti-GFP_VSV G
p=0.0081
Normalized GFP+%
Mock
Infected
Control
CD81 KO
CD63 KO
CD9 KO
D
Control
CD81 KO
p=0.0029
Dextran-555 MFI
Dextran
C
trVLP-dGP-GFP EBOV GP
trVLP-dGP-GFP VSV G
p=0.0248
p=0.0086
E
hCD81
p=0.0145
Normalized GFP+% (to BFP+%)
trVLP-dGP
trVLP-dGP EBOV GP

© The Author(s)

Figure 7. CD81 restricts early steps of EBOV trVLP infection.

(**A**) 293T control, CD81 KO, CD63 KO, and CD9 KO cells were mock or pre-transfected to express EBOV RNPs and Tim1 (EBOV attachment factor). One day later, the cells were infected with trVLP-GFP. 4 d.p.i., an aliquot of the cells was harvested for flow cytometry, and the remaining cells and medium were harvested for WB. Indicated are representative WB images and mean values (normalized to inf. control cells) of WB signal quantification and infection rate ± SD from $n = 4$ independent experiments. RM one-way ANOVA was used for statistical analysis. (**B**) 293T control, CD81 KO, CD63 KO, and CD9 KO cells were mock-infected or infected with lenti-GFP pseudotyped with EBOV GP or VSV G. 3 d.p.i., the cells were harvested for flow cytometry. Indicated are mean values of infection rate (normalized to infected control cells) ± SD from $n = 3$ (293T control/CD81 KO) or $n = 2$ (CD63/CD9 KO) independent experiments. (**C**) 293T control and KO cells were mock or pre- transfected to express EBOV RNP and Tim1. One day later, the cells were mock-infected or infected with trVLP-dGP-GFP pseudotyped with EBOV GP or VSV G. 3 d.p.i., cells were harvested for flow cytometry. Indicated are mean values of infection rate (normalized to infected control cells) ± SD from $n = 4$ (293T control/CD81 KO) or $n = 2$ (CD63/CD9 KO) independent experiments. (**D**) 293T control and CD81 KO cells were left untreated (mock) or incubated with Dextran-555 (10 K, 0.4 mg/ml). After incubation at 37 °C for 15 min, the cells were harvested for flow cytometry to analyze Dextran uptake. Indicated are mean values (normalized to control cells added with Dextran) of MFI ± SD from $n = 7$ independent experiments. (**E**) 293T WT cells were pre- transfected with plasmids expressing EBOV RNP, Tim1, and BFP and a CD81-HA expression plasmid or the control vector. One day later, cells were treated with trVLP-dGP-GFP or trVLP-dGP-GFP pseudotyped with EBOV GP. 48 h.p.i. cells were harvested for flow cytometry. Indicated are mean values of infection rate (normalized to BFP + % and further control infected cells) ± SD from $n = 3$ independent experiments. Welch's *t*-test was used for statistical analysis. Source data are available online for this figure.

Catalán et al, 2021). The functional relation of these findings to the restricting role of CD81 in the EBOV life cycle is not clear yet. Nevertheless, the data indicate that EBOV interferes with cell surface CD81 to avoid associated signaling, which results in an inhibitory activity on viral replication, involving NFκB. Findings that warrant further investigation.

Our study has certain limitations. First, the exact structural and functional motifs in GP, VP40 and CD81 that are involved in modulation and functional restriction remain largely elusive. Second, the restricting activity of CD81 on the EBOV life cycle was formally only demonstrated in the EBOV trVLP surrogate system of viral replication. Difficulties to assess the CD81 relevance in the context of authentic EBOV infection are due to the high potency of CD81-modulation by GP and VP40, which makes it challenging to draw conclusions when comparing EBOV infection in control vs CD81 KO cells. Nevertheless, a strong argument for CD81 also restricting authentic EBOV infection is the fact that we measure robust downmodulation of CD81 in the context of authentic EBOV infection, not only in 293T cells but also in primary human macrophages (Fig. 1D,F) and inhibition of authentic EBOV infection specifically by the CD81-targeting antibody (Fig. 8D,E). A finding that has certain translational potential that will be further followed up.

In summary, we identified novel EBOV GP-modulated plasma membrane proteins. Three of them are the tetraspanins CD81, CD63, and CD9 that are downregulated by highly divergent filovirus GPs. CD81, and not CD63 nor CD9, emerges as a cellular factor with inhibitory activity on EBOV entry and replication that is also interconnected to NFκB and therefore filoviral immunopathogenesis.

Methods

Reagents and tools table

Reagent/resource	Reference or source	Identifier or catalog number
Experimental models		
HEK293T cells (*H. sapiens*)	DSMZ	ACC 635
HeLa cells (*H. sapiens*)	DSMZ	ACC 57
Huh7.5 cells (*H. sapiens*)	R. Bartenschlager lab (Heidelberg)	N/A
HEK293T ctrl KO	This study	N/A
HEK293T CD81 KO	This study	N/A
HEK293T CD63 KO	This study	N/A
HEK293T CD9 KO	This study	N/A
Huh7.5 ctrl KO	This study	N/A
Huh7.5 CD81 KO	This study	N/A
Huh7.5 CD63 KO	This study	N/A
Huh7.5 CD9 KO	This study	N/A
Human monocyte-derived macrophages (MDMs)	Pseudonymized buffy coats of volunteer blood donors	N/A
Recombinant DNA		
pCG-3*-IRES-eGFP	Schindler et al (2003)	N/A
pCG-GPwt-IRES-GFP	Nehls et al, (2019)	N/A
pCG-IRES-GFP SEBOV-GP	Nehls et al, (2019)	N/A
pCG-IRES-GFP REBOV-GP	Nehls et al, (2019)	N/A
pCG-IRES-GFP CIEBOV-GP	Nehls et al, (2019)	N/A
pCG-IRES-GFP MARV-GP	Nehls et al, (2019)	N/A
pCG-IRES-GFP Lassa-GP	Nehls et al, (2019)	N/A
pCG-IRES-GFP NL4-3 Env	Nehls et al, (2019)	N/A
pLTR-PV	Braun et al (2019)	N/A
pLTR-EBL1-GP	Braun et al (2019)	N/A
pIAV_288_NA	Braun et al (2019)	N/A

© The Author(s)

Reagent/resource	Reference or source	Identifier or catalog number
pIAV_288_HA	Braun et al (2019)	N/A
pCG_SARS-CoV-2 S-IRES-GFP	Hagelauer et al (2023)	N/A
pCG_MERS S-IRES-GFP	M. Schindler lab (Tübingen)	N/A
pCG_SARS-CoV S-IRES-GFP	Hagelauer et al (2023)	N/A
pCAGGS_HIV-1_M_STCO-env	Boutin et al (2023)	N/A
pCAGGS_HIV-1_P_RBF168-env	Sauter et al (2011)	N/A
pMLV_env	Braun et al (2019)	N/A
pcDNA3_oricoHERV-K-env delta659-699-V5	Hanke et al (2009)	N/A
pCG-ZEBOV_GP1 -IRES-GFP	This study	N/A
pCG-ZEBOV_GP2 -IRES-GFP	This study	N/A
pCG-IRES-GFP SEBOV-GP1	This study	N/A
pCG-IRES-GFP SEBOV-GP2	This study	N/A
pCG-GP F88A-IRES-GFP	Nehls et al, (2019)	N/A
pCG-GP W104A-IRES-GFP	Nehls et al, (2019)	N/A
pCG-GP L111A-IRES-GFP	Nehls et al, (2019)	N/A
pCG-GP L122A-IRES-GFP	Nehls et al, (2019)	N/A
pCG ZEBOV GP 526I 528A-IRES-GFP	Nehls et al, (2019)	N/A
pCG ZEBOV GP 531 A 532 A 533A-IRES-GFP	Nehls et al, (2019)	N/A
pCG ZEBOV GP 535 A 536 A 537A-IRES-GFP	Nehls et al, (2019)	N/A
pCG ZEBOV GP 655 A 656A-IRES-GFP	Nehls et al, (2019)	N/A
pCG ZEBOV GP 666 A 667I 668A-IRES-GFP	Nehls et al, (2019)	N/A
pCG ZEBOV GP 670 A 672I-IRES-GFP	Nehls et al, (2019)	N/A
pCG-GP LxxxL-IRES-GFP	Nehls et al, (2019)	N/A
pCG-IRES-GFP ZLZ GP	Nehls et al, (2019)	N/A
pCG-IRES-GFP GP losh mut	Nehls et al, (2019)	N/A
pCG-IRES-GFP GP hish mut	Nehls et al, (2019)	N/A
pCG-IRES-GFP GPwt 2014	Nehls et al, (2019)	N/A
pCG-IRES-GFP GP V82A 2014	Nehls et al, (2019)	N/A
pCG-L-IRES-GFP	This study	N/A
pCG-NP-IRES-GFP	This study	N/A
pCG-VP35-IRES-GFP	This study	N/A
pCG-VP30-IRES-GFP	This study	N/A
pCG-VP40-IRES-GFP	This study	N/A
pCG-VP24-IRES-GFP	This study	N/A
pCAGGS-NP-v1.1	Watt et al, (2014)	N/A
pCAGGS-VP35-v1.1	Watt et al, (2014)	N/A
pCAGGS-VP30-v1.1	Watt et al, (2014)	N/A
pCAGGS-L-v1.1	Watt et al, (2014)	N/A
pCAGGS-T7opt	Watt et al, (2014)	N/A
pT7.1-4cis-vRNA-EBOV GP-nluc	Watt et al, (2014)	N/A
pT7.1-4cis-vRNA-dGP-nluc	This study	N/A
pPol II-4cis-vRNA-EBOV-GP-GFP	Schmidt et al, (2018)	N/A
pPol II-4cis-vRNA-dGP-GFP	This study	N/A
pCAGGS-Tim1-v1.2	Watt et al, (2014)	N/A
pCAGGS-luc2	Watt et al, (2014)	N/A
pCAGGS-MCS	S. Pöhlmann Lab (Göttingen)	N/A
pCAGGS ZEBOV GP wt	S. Pöhlmann Lab (Göttingen)	N/A
pCAGGS ZEBOV GPΔmuc	S. Pöhlmann Lab (Göttingen)	N/A
pCAGGS-Flag-EBOV VP40 wt	T. Hoenen Lab (Greifswald)	N/A
pVSV-G	Schindler et al (2003)	N/A
pWPI	Pham et al (2011)	N/A
pWPI_BLR	Banse et al (2018)	N/A
pWPI-hCD81-HAHA-BLR	Banse et al (2018)	N/A
mCherry-C1	J. Schmid Lab (Vienna)	N/A
pmtagBFP-C1	Suffner et al (2018)	N/A

© The Author(s)

Reagent/resource	Reference or source	Identifier or catalog number
pMD2G	Addgene	#12259
psPAX2	Addgene	#12260
lentiCRISPRv2	Addgene	#52961
lentiCRISPRv2-CD81	This study	5′- CATCGGCATTGCTGCCATCG-3′
lentiCRISPRv2-CD63	This study	5′- GAGGTGGCCGCAGCCATTGC-3′
lentiCRISPRv2-CD9	This study	5′- GCCCTCACCATGCCGGTCAA-3′
pSIV-vpr-vpx+	T. Gramberg lab (Erlangen)	N/A
pWPXLd	Addgene	#12258
phmKGN-MC	D. Sauter Lab (Tübingen)	N/A
phmKGN-MN	D. Sauter Lab (Tübingen)	N/A
phmKGC-MN	D. Sauter Lab (Tübingen)	N/A
pKGN_MC_NP	This study	N/A
pKGN_MN_NP	This study	N/A
pKGC_MN_NP	This study	N/A
pKGN_MC_VP35	This study	N/A
pKGN_MN_VP35	This study	N/A
pKGC_MN_VP35	This study	N/A
pKGN_MN_GP	This study	N/A
pKGC_MN_GP	This study	N/A
pKGN_MC_VP40	This study	N/A
pKGN_MN_VP40	This study	N/A
pKGC_MN_VP40	This study	N/A
pKGN_MC_CD81	This study	N/A
pKGN_MN_CD81	This study	N/A
pKGC_MN_CD81	This study	N/A
pEYFP-N1	Banning et al, (2010)	N/A
pmScarlet-C1	Addgene	#85042
mScarlet-YFP	J. Schmid Lab (Vienna)	N/A
pEYFP-N1 EBOV GP1/2	Kuhl et al, (2011)	N/A
pEYFP-N1 REBOV GP1/2	This study	N/A
pEYFP-N1 CIEBOV GP1/2	This study	N/A
pEYFP-N1 SEBOV-GP1/2	This study	N/A
pEYFP-N1 EBOV GP1	Kuhl et al, (2011)	N/A
pEYFP-N1 EBOV GP2	Kuhl et al, (2011)	N/A
pEYFP-C1 EBOV GP2	Kuhl et al, (2011)	N/A
pmScarlet-C1-CD81	M. Schindler lab (Tübingen)	N/A
pEYFP-C1 EBOV VP40	M. Schindler lab (Tübingen)	N/A
TGN-mScarlet	M. Schindler lab (Tübingen)	N/A
mScarlet-Clathrin	M. Schindler lab (Tübingen)	N/A
p_human IKKbeta, constitutively active mutant (S177E, S181E)	B. Baumann lab (Ulm)	N/A
pGL3-NF-κB F-Luc	B. Baumann lab (Ulm)	N/A
pCG_CH293_Vpu	D. Sauter Lab (Tübingen)	N/A
Antibodies		
PE anti-human CD357 Antibody	BioLegend	Cat. # 371203
PE anti-human CD79b Antibody	BioLegend	Cat. # 341404
PE anti-human HLA-A, B, C Antibody	BioLegend	Cat. # 311406
PE anti-human HLA-A, B, C Antibody	Milteny Biotec	Cat. # 130-120-055
PE anti-human CD59 Antibody	BioLegend	Cat. # 304707
PE anti-human CD257 Antibody	BioLegend	Cat. # 366505
PE anti-human CD9 Antibody	BioLegend	Cat. # 312105
APC anti-human CD9 Antibody	BioLegend	Cat. # 312108
PE anti-human CD276 Antibody	BioLegend	Cat. # 331605
PE anti-human CD24 Antibody	BioLegend	Cat. # 311105
PE anti-human CD81 Antibody (5A6)	BioLegend	Cat. # 349506
FITC anti-human CD81 Antibody (5A6)	BioLegend	Cat. # 349504
BV711 anti-human CD81 Antibody	BioLegend	Cat. # 740789
BV510 anti-human CD14 Antibody	BioLegend	Cat. # 301842
PE-Cy7 anti-human CD11b Antibody	BioLegend	Cat. # 301842
PE anti-human CD277 Antibody	Miltenyi Biotec	Cat. # 130-101-805
PE anti-human CD137L Antibody	BioLegend	Cat. # 311503
PE anti-human CD201 Antibody	BioLegend	Cat. # 351903
PE anti-human CD146 Antibody	BioLegend	Cat. # 342003

© The Author(s)

Reagent/resource	Reference or source	Identifier or catalog number
PE anti-human CD63 Antibody	BioLegend	Cat. # 353003
PE anti-human CD63 Antibody	BioLegend	Cat. # 353004
PE anti-human CD338 Antibody	BioLegend	Cat. # 332007
PE anti-human CD317 Antibody	BioLegend	Cat. # 348406
PE anti-human CD116 Antibody	BioLegend	Cat. # 305908
PE anti-human CD184 Antibody	BioLegend	Cat. # 306505
PE anti-human CD49c Antibody	BioLegend	Cat. # 343803
PE Mouse Anti-Human CD107a	BD Biosciences	Cat. # 555801
CD55 (DAF) Antibody, anti-human	Miltenyi Biotec	Cat. # 130-101-805
PE Mouse IgG1, κ Isotype Ctrl Antibody	BioLegend	Cat. # 400113
Mouse anti-EBOV VP40 mAb (3G5)	IBT Bioservices	Cat. # 0201-016
Rabbit anti-EBOV GP1	Nehls et al, (2019)	N/A
Polyclonal rabbit GP	Icosagen	Cat. # A2-100-100
Rabbit anti-CD81 antibody	Abcam	Cat. # ab219209
Goat anti-Mouse IgG (H + L) Cross-Adsorbed Secondary Antibody, Alexa Fluor™ 555	Thermo Fisher	Cat. # A-21422
CD81 Antibody (B-11)	Santa Cruz	Cat. # sc-166029
α-Tubulin Polyclonal Antibody	Thermo Fisher	Cat. # PA5-29444
Anti-GAPDH Antibody	BioLegend	Cat. # 607902
IRDye 680RD Goat anti-Mouse IgG	LI-COR	Cat. # 926-68070
IRDye 800CW Goat anti-Mouse IgG	LI-COR	Cat. # 926-32210
IRDye 680RD Goat anti-Rabbit IgG	LI-COR	Cat. # 926-68071
IRDye 800CW Goat anti-Rabbit IgG	LI-COR	Cat. # 926-32211
IRDye 800CW Goat anti-Rat IgG	LI-COR	Cat. # 926-32219
Anti-human CD81 Antibody, mouse (1.3.3.22)	Santa Cruz	# sc-7637
Duolink® In Situ PLA® Probe Anti-Rabbit PLUS	Sigma-Aldrich	DUO92002-30RXN
Duolink® In Situ PLA® Probe Anti-Mouse MINUS	Sigma-Aldrich	DUO92004-30RXN
Rabbit anti-EBOV NP pAb	Gentaur	Cat. # 4940301-012
Goat anti-Rabbit IgG, Alexa Fluor594	Thermo Fisher	Cat. # A-11012
Rabbit anti-p65	Cell Signaling	Cat. # 8242
Anti-human CD81 Antibody (5A6)	BioLegend	Cat. # 349502
Mouse IgG1, κ Isotype Ctrl Antibody	BioLegend	Cat. # 400102
Oligonucleotides and other sequence-based reagents		
qPCR hGAPDH fw	Businger et al (2019)	TGCACCACCAACTGCTTAGC
qPCR hGAPDH rv	Businger et al (2019)	GGCATGGACTGTGGTCATGAG
qPCR hCD81 fw	Chang et al (2016)	AGGGCTGCACCAAGTGC
qPCR hCD81 rv	Chang et al (2016)	TGTCTCCCAGCTCCAGATA
qPCR Fluc fw	Wendt et al (2020)	CAGTCGTCGTGCTGGAACAC
qPCR Fluc rv	Wendt et al (2020)	GTCCAACTTGCCGGTCAGTC
qPCR EBOV VP40 fw	Shabman et al (2013)	TCCCGGATCATCCCCTCAGGC
qPCR EBOV VP40 rv	Shabman et al (2013)	GCAGCAGGCAGTGGTTGGGT
EBOV vRNA	Chen et al, (2019)	ATTGAAGATTCAACAACCCTAAAG
EBOV cRNA	Chen et al, (2019)	AATATGAGCCCAGACCTTTCG
Chemicals, enzymes and other reagents		
Duolink® In Situ Detection Reagents Red	Sigma-Aldrich	Cat. # DUO92008
Q5 High-Fidelity DNA Polymerase	New England Biolabs	Cat. # M0491S
T4 DNA Ligase	Thermo Fisher	Cat. # EL0011
MG132	AdipoGen Life Sciences	Cat. # AG-CP3-0011-M001
Bafilomycin A1	AdipoGen Life Sciences	Cat. # AG-CN2-2001-C100
PMA	Sigma-Aldrich	Cat. # p1585
Dextran, Alexa Fluor 555; 10,000 MW	Thermo Fisher	Cat. # D34679
PNGase F	Promega	Cat. # V4831
Puromycin	Sigma-Aldrich	Cat. # P8833
Ficoll-Paque Plus	Sigma-Aldrich	Cat. # GE17-1440-03
Human AB serum	Sigma-Aldrich	Cat. # H4522

© The Author(s)

Reagent/resource	Reference or source	Identifier or catalog number
Polyethylenimine, Linear, MW 25000, Transfection Grade	Polysciences	Cat. # 23966
JetPRIME DNA and siRNA Transfection Reagent	Polyplus	Cat. # 101000001
Lipofectamine2000	Thermo Fisher	Cat. # 11668019
DharmaFECT™ siRNA transfection reagent	Horizon Discovery	Cat. # T-2004
Accutase	BioLegend	Cat. # 423201
BD Cytofix Fixation Buffer	BD Biosciences	Cat. # 554655
Software		
GraphPad Prism 9.4.1/11.0.1	https://www.graphpad.com/	
ImageJ	https://imagej.net/ij/index.html	
FlowLogic	https://www.inivai.com/flowlogic	
FlowJo v10	https://www.flowjo.com/flowjo10/overview	
SerialCloner 2.6.1	http://serialbasics.free.fr/Serial_Cloner.html	
Image Studio Software	https://www.licorbio.com/image-studio	
Incucyte Software 2022B	https://www.sartorius.com/en/products/live-cell-imaging-analysis/live-cell-analysis-software	
Other		
Luna Universal qPCR Master Mix	New England Biolabs	Cat. # M3003
Nano-Glo Luciferase Assay System	Promega	Cat. # N1110
Firefly-Luciferase Assay System	Promega	Cat. # E1500
RNeasy Mini Kit	Qiagen	Cat. # 74104
QuantiTect Reverse Transcription kit	Qiagen	Cat. # 205311
LEGENDScreen™ Human Cell PE Kit	BioLegend	Cat. # 700007
CoralHue® Fluo-chase Kit	MBL Life Science	Cat. # AM-1100M

Cell culture

293T and HeLa cells were cultured in DMEM with 10% FCS and 1% Penicillin/Streptomycin (P/S). Huh7.5 cells were cultured in DMEM with 10% FCS, 1% non-essential amino acid (NEAA), 1% sodium pyruvate, and 1% P/S. CD81 KO, CD63KO, CD9KO, and the control cells were cultured in medium containing 1 µg/ml puromycin. All cells were regularly screened for mycoplasma and found to be negative. Human monocyte-derived macrophages (MDM) were prepared from PBMCs essentially as described in (Businger et al, 2021). PBMCs were isolated from blood samples via Ficoll-Paque gradient centrifugation, and macrophages were differentiated from PBMCs in macrophage medium (RPMI + 4% human AB serum + 1% NEAA + 1% sodium pyruvate + 1% P/S + 0.4% MEM vitamins). The cells were cultured in an incubator with 5% CO_2 and 90% relative humidity at 37 °C. MDMs were generated from pseudonymized buffy coats of volunteer blood donors. Blood donors give informed consent for the use of blood and blood-derived products for research use. We do not collect data concerning age and ethnicity, and we comply with all relevant ethical regulations approved by the ethics committee of the University Hospital Tübingen (IRB no. 507/2017B01 and 612/2020 A). All buffy coat donations are received in pseudonymous form and chosen randomly.

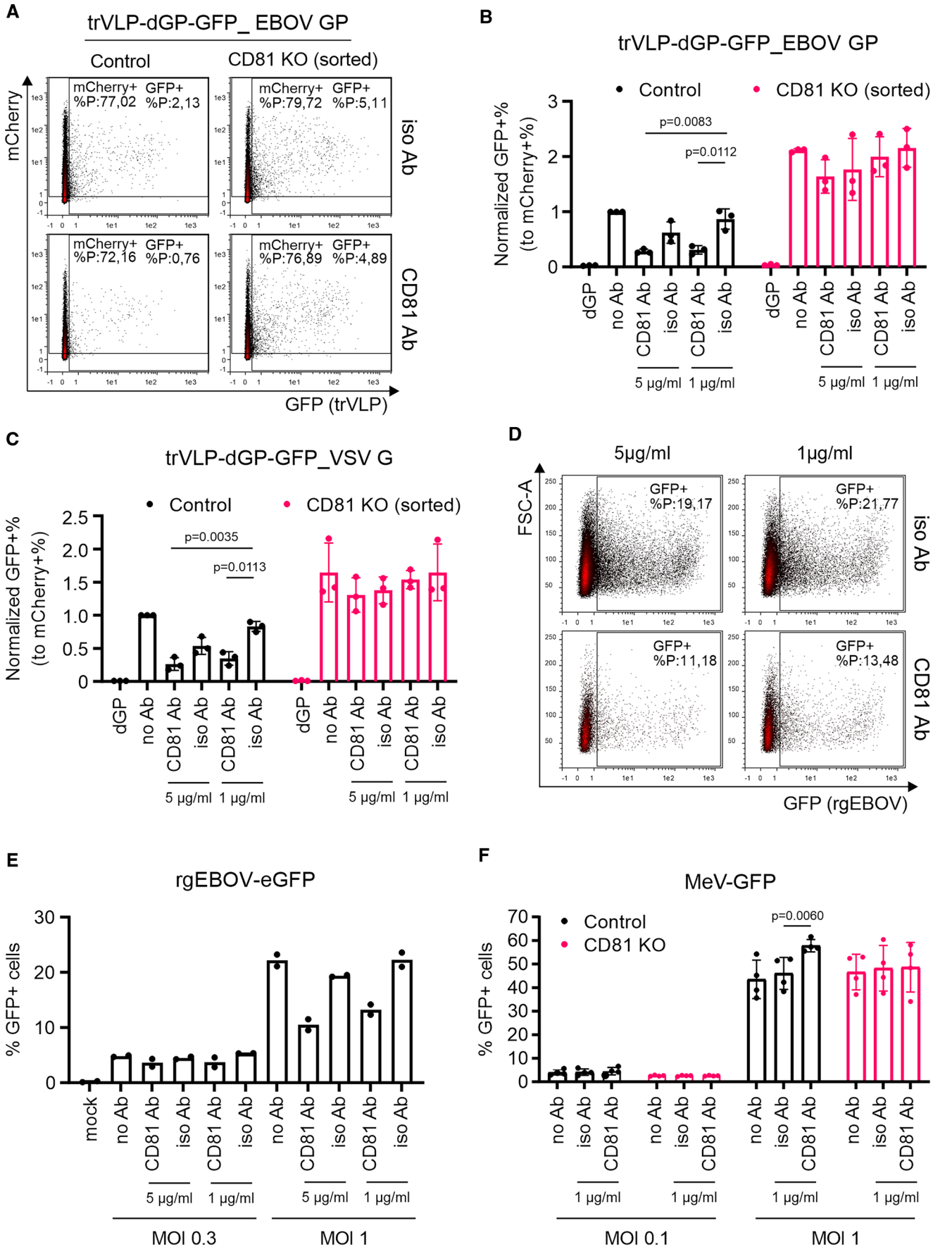
Plasmids and antibodies

Plasmids and antibodies used in this study are listed in the Reagents and Tools table. EBOV NP, L, VP35, VP30, VP40, and VP24 were ligated into pCG-3*-IRES-eGFP using XbaI and MluI. The plasmids for the trVLP assay were described before (Watt et al, 2014). EBOV RNA polymerase II driven tetracistronic minigenome plasmid with a GFP reporter is described here (Schmidt et al, 2018). Plasmids expressing EBOV GP, VP40, NP and VP35 as well as CD81 fused with the N/C part of Kusabira-green (KG) protein were generated by using BamHI and NotI restriction sites.

Transfection

Calcium phosphate was used for the transfection of 293T cells. In a six-well plate format, 5 µg plasmids and 13 µl 2 M $CaCl_2$ were mixed with H_2O in a total volume of 100 µl. The DNA mixture was added dropwise to 100 µl of cold 2× HBS while vortexing. After vortexing for an additional 10 s, the transfection mixture was incubated on ice for 15 min and added dropwise to the cells. Six hours later, the medium was replaced with fresh medium. Polyethylenimine (PEI) was also used for the transfection of 293T cells. In a 12-well plate format, 1 µg plasmids were mixed with 50 µl Opti-MEM, and 3 µl of 1 µg/µl PEI was mixed with 50 µl Opti-MEM. The PEI mixture was added to the plasmid mixture and mixed by pipetting. After incubation at RT for 15 min, the transfection mixture was added dropwise to the cells. 16 h later (o/n), the medium was replaced with fresh medium. For transfection of other formats, the amount of plasmid and PEI was adjusted accordingly. JetPRIME (PolyPlus) was used for transfection of 293T, HeLa and Huh7.5 cells according to the

© The Author(s)


A
trVLP-dGP-GFP_ EBOV GP
Control
CD81 KO (sorted)
mCherry
mCherry+ GFP+
%P:77,02 %P:2,13
mCherry+ GFP+
%P:79,72 %P:5,11
mCherry+ GFP+
%P:72,16 %P:0,76
mCherry+ GFP+
%P:76,89 %P:4,89
iso Ab
CD81 Ab
GFP (trVLP)
B
trVLP-dGP-GFP_EBOV GP
Control
CD81 KO (sorted)
Normalized GFP+%
(to mCherry+%)
p=0.0083
p=0.0112
dGP
no Ab
CD81 Ab
iso Ab
5 µg/ml
1 µg/ml
C
trVLP-dGP-GFP_VSV G
Control
CD81 KO (sorted)
Normalized GFP+%
(to mCherry+%)
p=0.0035
p=0.0113
D
5µg/ml
1µg/ml
FSC-A
GFP+
%P:19,17
%P:21,77
%P:11,18
%P:13,48
iso Ab
CD81 Ab
GFP (rgEBOV)
E
rgEBOV-eGFP
% GFP+ cells
mock
MOI 0.3
MOI 1
F
MeV-GFP
Control
CD81 KO
p=0.0060
% GFP+ cells
MOI 0.1
MOI 1

© The Author(s)

Figure 8. CD81 antibody treatment inhibits EBOV trVLP and authentic EBOV infection.

(**A–C**) 293T control and CD81 KO cells were pre-transfected to express EBOV RNP, Tim1, and mCherry. One day later, the cells were mock-treated or treated with the CD81 antibody (5A6) or the corresponding isotype antibody. After 1 h incubation, the cells were infected with trVLP-dGP-GFP or trVLP-dGP-GFP pseudotyped with EBOV GP (**A**, **B**) or VSV G (**C**). 2 d.p.i., cells were harvested for flow cytometry. Shown are (**A**) representative density plots and (**B**, **C**) mean values of infection rate (normalized to mCherry+ % and further no Ab treated control cells) ± SD from $n = 3$ independent experiments. (**D**, **E**) 293T cells were treated with no Ab, CD81 antibody (5A6) or the corresponding isotype antibody. 1 h later, the cells were mock-infected or infected with rgEBOV-GFP at MOI 0.3 or 1. 1 d.p.i., cells were harvested and fixed for flow cytometry. Shown are (**D**) representative density plots and (**E**) mean values of infection rate (GFP + %) from $n = 2$ independent experiments, performed in technical duplicates. (**F**) As specificity control, 293T control and CD81 KO cells were treated with no Ab, CD81 antibody (5A6) or the corresponding isotype antibody and infected 1 h later with MeV-GFP at MOI 0.1 or 1. 2 d.p.i., cells were harvested and fixed for flow cytometry. Shown are mean values of infection rate (GFP + %) ± SD from $n = 4$ independent experiments. (**B**, **C**, **F**) Two-way ANOVA with Fisher's LSD was used for statistical analysis. Source data are available online for this figure.

manufacturer's protocol. DharmaFECT 4 transfection reagent was used for transfection of human primary macrophages with ON-TARGETplus human CD81 siRNA–SMARTPool or ON-TARGETplus non-targeting control siRNA #2 according to the manufacturer's recommended protocol.

Generation of knockout (KO) cells

293T CD81 KO cells were generated via lentiviral transduction. 293T cells in six-well plates were transfected with 0.45 µg pVSV-G, 1.125 µg psPAX2, and 1.5 µg lentiCRISPRv2-CD81 to produce lentiviruses carrying Cas9 and a gRNA targeting CD81. In parallel, 293T cells were transfected with 2.5 µg pSIV-vpr-vpx+ and 0.25 µg pVSV-G to produce Vpx-VLPs, which were used to knock down SAMHD1 in target cells to improve lentiviral transduction efficiency (Gramberg et al, 2013). Twenty-four hours later, the supernatants containing lentiviruses and Vpx-VLPs were collected and centrifuged at 3200×*g* for 10 min to remove dead cells and cell debris. The cleared supernatants were collected for transduction. 293T cells seeded in six-well plates were treated with Vpx-VLPs for 2 h and infected with lentiviruses for 24 h. Twenty-four hours later, the cells were cultured in medium with 1 µg/ml puromycin for selection of successfully transduced cells. 293T control, CD63 KO and CD9 KO cells were generated by transfection of 293T cells in six-well plates with 0.45 µg pMD2G, 1.125 µg psPAX2, and 1.5 µg lentiCRISPRv2, lentiCRISPRv2-CD63, or lentiCRISPRv2-CD9. One week later, the cells were cultured in medium containing 1 µg/ml puromycin. After selection, the KO efficiency of the cells was analyzed by flow cytometry. 293T CD81 KO cells stained with PE-conjugated anti-human CD81 antibody were subjected for fluorescence-activated cell sorting (FACS), PE mouse IgG1, κ isotype ctrl antibody stained 293T CD81 KO cells were used for gating. Collected 293T CD81 KO cells from FACS are termed 293T CD81 KO cells (sorted).

Legend screen

HeLa cells were transfected with pCG-GPwt-IRES-GFP to coexpress EBOV GP and GFP. Thirty-six hours later, using the LEGENDScreen™ Human Cell PE Kit, the cells were harvested and stained with antibodies against 332 receptors and ten isotype ctrl antibodies according to the manufacture's protocol and in detail as previously described (Businger et al, 2021; Heumos et al, 2022). The primary data is accessible through Dataset EV1.

Flow cytometry staining

Surface staining was performed with 293T, HeLa, Huh7.5 cells, and human primary monocyte-derived macrophages (MDM). The cells were stained with PE-conjugated antibodies diluted in FACS buffer (1% FCS in PBS) for 30 min at 4 °C in the dark. FACS buffer was added to the cells for washing. The cells were centrifuged at 600×*g* for 5 min, and the washing step with FACS buffer was repeated once. Subsequently, the cells were either resuspended in FACS buffer for direct measurement or fixed with 2% paraformaldehyde (PFA). For staining of EBOV-infected 293T cells or MDMs, the cells were fixed as described in EBOV infection before staining. For the PNGase assay, cells were treated 24 h.p.t. for 4 h with 100 U/ml PNGase F (Promega) at 37 °C, before harvesting and staining for flow cytometry.

For intracellular staining, 2% PFA fixed (15 min at RT) surface-stained cells were washed with PBS and permeabilized with ice-cold 90% methanol (in H_2O, stored at −20 °C) at 4 °C for 20 min. PE of surface-stained antibodies is damaged by methanol (Krollmann et al, 2022). After the permeabilization, the cells were washed with FACS buffer and blocked with 10% FCS (in PBS) for 30 min at RT. The cells were then stained with PE-conjugated antibodies and washed twice with FACS buffer. For total staining, fixed surface-stained cells were washed with PBS and permeabilized with 0.2% saponin for 10 min at RT. The cells were then blocked with 10% FCS in 0.2% saponin for 30 min at RT. After washing with FACS buffer, the cells were stained with PE-conjugated antibodies and washed twice with FASC buffer. For total staining of fixed EBOV-infected 293T cells, the cells were permeabilized, blocked, stained and washed as described for the intracellular staining.

The measurements were done with the MACSquant VYB (Miltenyi Biotec). For tetraspanin modulation in rgEBOV-GFP-infected MDMs, the 5 L Cytek Aurora (Cytek Biosciences) was used. The flow cytometry gating strategy is detailed in Figs. EV1 and 1. For several analysis we included gates of intermediate (GFP/GP+) and high (GFP/GP++) GP-expressing cell populations. These gates are defined within each experiment based on the GFP distribution relative to the matched non-GFP expressing control and applied consistently across the corresponding samples.

Microscopy and immunofluorescence

For assessment of inclusion body (IB) formation, 1×10^5 293T control and CD81 KO cells were seeded in poly-L-lysine-coated thin-bottom plates in a 24-well format. The following day, the cells were transfected using PEI with a total of 0.4 µg of DNA. The cells were fixed 24 h post transfection (h.p.t.) with 2% PFA for 15 min at

© The Author(s)

Table 1. PLA antibodies

Antibody	Dilution	Manufacturer
Polyclonal rabbit GP	1:100	Icosagen # A2-100-100
Anti-human CD81 Antibody (5A6)	1:100	BioLegend # 349502
Mouse anti-EBOV VP40 mAb (3G5)	1:100	IBT Bioservices # 0201-016
Rabbit anti-CD81 antibody	1:100	Abcam # ab219209

RT. After two washing steps with PBS, the cells were permeabilized with 0.2% saponin in PBS for 10 min and subsequently blocked with 10% normal goat serum (NGS) for 1 h at RT. After three washes with PBS, the cells were incubated with the primary antibody for 1 h at RT. Following three additional washes with PBS, the cells were stained with the fluorescently labeled secondary antibody for another hour at RT. Antibody dilutions were prepared in 0.1% saponin in FACS buffer (1% FCS in PBS). To visualize cell nuclei, cells were stained with DAPI (0.1 µg/ml in PBS) for 10 min at RT. After two final washes, images were acquired using the Cytation3 imaging microplate reader at 40x magnification. IBs were quantified as red object count using ImageJ software.

For p65 detection, 2×10^4 293T control and CD81 KO cells were seeded into a poly-L-lysine-coated 96-well plate and transfected the next day using jetPRIME. 6 h.p.t., the medium was replaced, and the cells were infected with EBOV trVLP-dGP-GFP. 48 h.p.t., the cells were fixed with 2% PFA for 15 min at RT, washed twice with PBS, and incubated for 5 min with a permeabilization and blocking buffer (5% FCS and 0.5% Triton X-100 in PBS). The cells were washed with PBS and incubated with the primary antibody for 1 h at RT. After washing with PBS, the cells were stained with the secondary antibody for 1 h at RT. Nuclei were stained with DAPI (0.1 µg/ml in PBS) for 10 min at RT. The staining procedure concluded with another wash with PBS, and cells were imaged using the Cytation3 at 4x magnification. For quantification using ImageJ, a green mask was generated to identify GFP-positive cells (transfected or infected cells), and the red mean fluorescence intensity (p65 staining) within the green mask was measured.

For assessment of CD81, EBOV GP, and VP40 localization, HeLa cells were seeded in µ-Slide 8-well high glass bottom IBID plates (2×10^4 cells per well). One day later, they were transfected using the jetPRIME buffer, and the medium was changed after 4 h. 24 h.p.t., cells were fixed with 2% PFA, permeabilized with 0.2% saponin and blocked and stained as described before for IB formation detection. Cells were imaged using the ZEISS Apotome 3 fluorescent microscope at 63x magnification.

Proximity-ligation assay (PLA)

PLA staining was performed essentially according to the manufacturer's instructions using the Duolink® PLA kit, with minor adaptations as indicated. HeLa cells were seeded at a density of 5×10^4 cells/well in a 12-well plate onto cover slips. The next day, cells were transfected with GFP alone, or EBOV GP or VP40 together with GFP from a bicistronic mRNA using jetPRIME and 0.8 µg plasmid DNA per well. After an incubation period of 4 h, the medium was changed to fresh medium. 24 h.p.t., cells were fixed using 2% PFA and subsequently permeabilized with 0.2% saponin. After blocking cells o/n with 10% NGS, cells were incubated in a humidity chamber with primary antibodies for 1 h at RT. For PLA background control, GFP-only samples corresponding to the GP-CD81 and VP40-CD81 conditions were stained with the same primary antibodies as the respective PLA samples. During incubation with primary antibodies (see Table 1), PLA probes were diluted 1:5 in 1% FCS in PBS and incubated for 20 min at RT. After washing cells 2x with wash buffer A, PLA probes were added to the cells and incubated in a humidity chamber at 37 °C for 1 h. Afterward, cells were again washed 2x with wash buffer A and further incubated with ligation solution in a humidity chamber at 37 °C for 30 min. Subsequently, amplification solution was added to the cells and further incubated at 37 °C for 100 min. Cells were then washed with wash buffer B and dried on a tissue. Cover slips were mounted on microscopic slides and analyzed using the DeltaVision™ OMX SR system. For quantification, GFP-positive (transfected) cells were segmented in ImageJ to generate individual cell masks, and PLA spots were counted within each mask using the particle analysis tool.

Flow cytometry-based-FRET

The experiment was essentially performed as described in (Banning et al, 2010; Kuhl et al, 2011). 293T cells were seeded in a 12-well plate format using 3×10^5 cells per well and transfected the next day using PEI. For transfection, a YFP-fusion protein was co-transfected with an mScarlet-fusion protein and the cells were harvested 24 h.p.t. for flow cytometry analysis. YFP was excited using the 488 nm laser and detected with a 525/50 nm band pass filter. FRET signal was measured by excitation with the 488 nm laser and detection using a 614/50 nm filter. For the exclusion of false positive FRET signal, mScarlet was excited with a 561 nm laser and detected using a 615/20 nm filter.

Western blot

The cells were lysed with RIPA buffer (140 mM NaCl, 10 mM Tris-HCl, 1 mM EDTA, 0.5 mM EGTA, 0.1% (w/v) Na-deoxycholate, 0.1% (w/v) SDS, 1% (v/v) Triton X-100 in H_2O, pH 7.4) with freshly-added protease inhibitor at 4 °C for at least 20 min. The cell lysates were centrifuged at 20,000×*g* for 10 min at 4 °C, and supernatants were taken and mixed with 5× Laemmli buffer. The medium containing trVLPs was cleared by centrifugation at 3200×*g* for 10 min and the supernatants containing VLPs were taken and top layered on 20% sucrose. The VLPs were pelleted by centrifugation at 20,000×*g* for 90 min at 4 °C and suspended in 1× Laemmli buffer (diluted with RIPA buffer). After mixing with Laemmli buffer, the cell lysates and VLPs were incubated at 95 °C for 10 min. 12 or 15% acrylamide gels were used for SDS-PAGE. When CD81 was detected, 15% gel was used. The proteins were transferred to PVDF membranes, followed by blocking with 5% milk in TBS for at least 1 h. The membranes were incubated with primary antibodies at 4 °C o/n or at RT for 2–3 h and washed with TBS-T (0.1% Tween-20 in TBS) 3× 10 min. Secondary antibodies were incubated with the membranes in the dark for 1 h at RT and washed with TBS-T three times. Detection was performed using the Odyssey Fc Imaging System.

© The Author(s)

Table 2. Transfection scheme to produce trVLP-nluc and trVLP-dGP-nluc

Plasmid	Mass (μg)-scheme 1	Mass (μg)-scheme 2
pCAGGS-NP-v1.1	0.125	0.0625
pCAGGS-VP35-v1.1	0.125	0.0625
pCAGGS-VP30-v1.1	0.075	0.0375
pCAGGS-L-v1.1	1	0.5
pCAGGS-T7opt	0.25	0.125
pT7.1-4cis-vRNA-EBOV GP-nluc or pT7.1-4cis-vRNA-dGP-nluc	0.25	0.125

Table 3. Transfection scheme to produce trVLP-GFP and trVLP-dGP-GFP

Plasmid	Mass (μg)-scheme 1	Mass (μg)-scheme 2
pCAGGS-NP-v1.1	0.125	0.0625
pCAGGS-VP35-v1.1	0.125	0.0625
pCAGGS-VP30-v1.1	0.075	0.0375
pCAGGS-L-v1.1	1	0.5
pPol II-4cis-vRNA-EBOV GP-GFP or pPol II-4cis-vRNA-dGP-GFP	0.25	0.125

trVLP luciferase assay

The cells were lysed with 200 μl luciferase lysis buffer (25 mM glycylglycine (pH 7.8), 15 mM $MgSO_4$, 4 mM EGTA, 10% (v/v) glycerol, 1% (v/v) Triton X-100, and 1 mM DTT (before use) in H_2O) at RT for 15 min. For the firefly-luciferase (Fluc) assay, 40 μl Fluc assay buffer (0.1 M KH_2PO_4/K_2HPO_4, pH 7.8, 15 mM $MgSO_4$, and 5 mM ATP in H_2O) was added to opaque white 96-well plates and mixed with 40 μl cell lysates and 40 μl Fluc substrate buffer (0.28 mg/ml D-Luciferin in Fluc assay buffer). For the NanoLuc luciferase (Nluc) assay, Nluc substrate buffer was prepared by diluting Nluc substrate in Nluc assay buffer at a ratio of 1/50 according to the manufacture's protocol (Nano-Glo Luciferase Assay System). About 40 μl cell lysate was added to opaque white 96-well plates and mixed with 40 μl Nluc substrate buffer. The measurements were done with the Cytation3 Cell Imaging Multi-Mode Reader.

NFκB luciferase assay

A luciferase reporter plasmid was used for analysis of NFκB activity, followed by firefly-luciferase signal detection using the luciferase assay system of Promega (#E1500). 293T cells seeded in a 96-well format (2.5×10^4 cells/well) were transfected with 0.1 μg of NF-κB reporter plasmid (pGL3-NF-κB F-Luc), 0.05 μg of potential NFκB activator (EBOV proteins or constitutively active mutant of IKKβ) and, for the CD81 titration experiment, an additional of 0.1 μg of control or CD81-encoding pWPI plasmid. 24 h.p.t., cells were lysed with 40 μl of 1x Cell Lysis Buffer (diluted in H_2O) for 5 min at RT. 30 μl of cell lysate was mixed with 30 μl luciferase substrate in a white 96-well plate and relative light units per second (RLU/s) were measured in the Berthold microplate reader.

RT-qPCR

RNAs were extracted from the cells with RNeasy Mini Kit with on-column DNase digestion (Qiagen). About 1 μg RNA was used for reverse transcription with QuantiTect Reverse Transcription kit (Qiagen). For transcription of EBOV minigenome vRNA and cRNA, specific primers were used, vRNA: ATTGAAGATTCAA-CAACCCTAAAG, cRNA: AATATGAGCCCAGACCTTTCG) (Chen et al, 2019). Oligo(dT) (Thermo Fisher) was used for reverse transcription of mRNA. After reverse transcription, the reaction mixture (20 μl) was diluted with 40 μl RNase free water, and 5 μl diluted reverse transcription mixture was used for qPCR. qPCR reactions were prepared with Luna Universal qPCR Master Mix (New England Biolabs) and 0.3 μM (final concentration) primers. Measurements were done with LightCycler 480 System. qPCR results were analyzed using the ΔΔCp method (Pfaffl, 2001).

BiFC assay

Kusabira-green (KG) based bimolecular fluorescence complementation (BiFC) assay from MBL life science (CoralHue® Fluo-chase Kit, a gift from AG Sauter) was used to analyze protein-protein interaction. 293T cells in 96-well plates were transfected with 75 ng KGN expression plasmids and 75 ng KGC expression plasmids. In the assay to analyze whether CD81 interacts with NP in the presence of VP35, 50 ng KGN expression plasmids and 50 ng KGC expression plasmids were transfected together with 50 ng pCAGGS-VP35_v1.1. 2 days post transfection, the cells were harvested and surface stained with PE-conjugated CD81 antibody for flow cytometry.

Production and infection of lentivirus pseudotypes

To produce EBOV GP or VSV G pseudotyped GFP expressing lentiviruses, 293T cells in six-well plates were transfected with 1.125 μg psPAX2, 1.5 μg pWPXLd, and 0.125 μg pVSV-G or pCAGGS ZEBOV GP wt using PEI. After incubation o/n, the medium was changed and medium containing lentivirus pseudotypes was harvested 3 days later. The lentivirus-containing medium was cleared by centrifugation at 3200×*g* for 10 min. About 0.9 ml of cleared medium was used for infection of 293T cells in 12-well plates and the medium was changed one day post infection. Three days post infection, the cells were harvested and fixed with 2% PFA for flow cytometry.

EBOV trVLP assay

The EBOV trVLP production and infection assay was performed according to (Watt et al, 2014). 293T cells in 12-well plates were transfected according to Table 2 scheme 1 to produce trVLP-nluc and trVLP-dGP-nluc using PEI, and the medium was changed after o/n incubation. To produce trVLP-nluc and trVLP-dGP-nluc in Huh7.5 cells, half the amount of the plasmids (Table 2 scheme 2) was transfected using jetPRIME, and the medium was changed 4 h post transfection. 3 d.p.t., the cells were harvested for WB. In CD81 restoration experiments, 293T CD81 KO cells in 12-well plates were pre-transfected with pWPI-hCD81-HAHA-BLR (0, 0.0625, 0.125, 0.25, 0.5, and 1 μg) together with pWPI (1, 0.9375, 0.875, 0.75, 0.5, and 0 μg) in a total of 1 μg plasmids 1 day before transfection to

© The Author(s)

Table 4. Transfection scheme for trVLP infection

Plasmid	Mass (µg)-scheme 1	Mass (µg)-scheme 2
pCAGGS-NP-v1.1	0.125	0.0625
pCAGGS-VP35-v1.1	0.125	0.0625
pCAGGS-VP30-v1.1	0.075	0.0375
pCAGGS-L-v1.1	1	0.5
pCAGGS-Tim1-v1.2	0.25	0.125

produce trVLPs. Table 2 scheme 2 and 0.05 µg pCAGGS-luc2 (transfection ctrl) were transfected to produce trVLP-nluc or trVLP-dGP-nluc, half of the cells were harvested for WB and half of the cells were prepared for luciferase assay (3 d.p.t.). Amounts indicated in Table 3 scheme 2 were transfected to produce trVLP-GFP or trVLP-dGP-GFP, and the cells were harvested for WB (3 d.p.t.). For live cell imaging experiments, cells in 96-well plates (triplicates) were transfected with 1/10 of scheme 2 (Table 3) together with 0.05 µg (10×) mCherry-C1 (transfection control). Live cell imaging started 6 h post transfection after medium change. For qPCR experiments, Table 2 scheme 1 and 0.1 µg pCAGGS-luc2 were transfected, and the cells were harvested 3 days post transfection.

To produce trVLP-GFP for infection, 293T cells in six-well plates were transfected as indicated in Table 3 scheme 1 (pPol II-4cis-vRNA-EBOV GP-GFP). After incubation o/n, the medium was changed and trVLP-GFP containing medium was harvested 3 days post transfection. The trVLP-containing medium was clarified by centrifugation at 800×*g* for 5 min and supernatants were used for infection. The produced trVLPs were passaged twice and used for infection of target cells in the experiments. To produce trVLP-dGP-GFP pseudotyped with EBOV GP or VSV G (trVLP-dGP-GFP_EBOV GP or VSV G) for infection, 293T cells in six-well plates were transfected with 2× scheme 1 (pPol II-4cis-vRNA-dGP-GFP) and 0.125 µg (2×) pCAGGS ZEBOV GP wt or pVSV-G. After incubation for 4 h or o/n, the medium was changed and VLP-containing medium was harvested 3 days later. The VLP-containing medium was centrifuged at 3200×*g* for 10 min and supernatants were taken for infection. For trVLP-GFP infection, 293T cells in 12-well plates were pre-transfected as scheme 1 (Table 4) one day before infection. About 1 ml of cleared trVLP-GFP containing medium was added to the cells and medium was changed 1 day later. Three days post infection, the cells and medium were harvested. 1/5 cells were collected for flow cytometry, and the remaining cells and medium were prepared for WB. For infection with trVLP-dGP-GFP_EBOV GP or VSV G (Fig. 7C), 293T cells in 12-well plates were pre-transfected with EBOV ribonucleoprotein complex (RNP) (NP, VP35, VP30, and L) and Tim1 as indicated in scheme 1 (Table 4) and 0.1 µg pCAGGS-luc2 (transfection ctrl, optionally) was co-transfected 1 day before infection. The cells were infected with 0.9 ml of cleared trVLP-dGP-GFP_EBOV GP or VSV G for 1 day and the medium was changed. 3 days post infection, the cells were harvested for flow cytometry. For infection of 293T cells with trVLP-dGP-GFP_EBOV GP with 293T wt cells (Fig. 7E), the cells in 96-well plates (triplicates) were pre-transfected with 1/10 scheme 2 (Table 3) + 0.05 µg (10×) pmtagBFP-C1 (transfection control) + 0.5 µg (10×) pWPI-hCD81-HAHA-BLR or pWPI_BLR. In case of Tim1-, pCAGGS-MCS instead of pCAGGS-Tim1-v1.2 was transfected. One day later, the cells were infected with 100 µl clarified trVLP-dGP-GFP_EBOV GP for 1 day, followed by medium change. Two days post infection, the cells were harvested and surface stained with PE-conjugated CD81 antibody for flow cytometry. In the CD81 antibody treatment experiment, 293T cells seeded in 96-well plates (triplicates) were pre-transfected 1/10 of scheme 2 (Table 4) and 0.05 µg (10×) mCherry-C1. 1 day later, the medium was removed from the cells and 60 µl medium containing no antibody, 10 or 2 µg/ml anti-human CD81 Antibody (5A6) or Mouse IgG1, κ Isotype Ctrl Antibody was added. One hour later, the cells were infected with 60 µl cleared trVLP-dGP-GFP, trVLP-dGP-GFP_EBOV GP, or VSV G. 2 days post infection, the cells were harvested for flow cytometry. For flow cytometry, the cells were either fixed with 2% PFA or directly measured.

EBOV infection

293T control cells in six-well plates were infected with rgEBOV-eGFP (Hoenen et al, 2013) at an MOI of 1. Monocyte-derived macrophages (MDM) were generated as described in cell culture section and seeded in 6-well plates with a density of 9×10^4 cells per well. MDMs were infected the following day at an MOI of 0.5. Twenty-four hours post infection (h.p.i.) (293T) or 6 d.p.i. (MDM), the cells were harvested using Accutase (BioLegend) and fixed with 4% PFA at 4 °C for at least 24 h or using BD Cytofix Fixation Buffer (BD Biosciences) at RT for at least 1 h. Subsequently, the cells were washed with PBS and stained with PE-conjugated antibodies against CD81, CD63 and CD9 for flow cytometry. In the experiment with the CD81 antibody (5A6) treatment, 293T cells in 12-well plates were treated with no antibody (medium only), 5 or 1 µg/ml anti-human CD81 Antibody (5A6) or Mouse IgG1, κ Isotype Ctrl Antibody. 1 h later, the cells were infected with rgEBOV-GFP at a MOI of 0.3 or 1, with the virus diluted in medium containing or lacking antibody, as appropriate. Twenty-four hours post infection, the cells were harvested and fixed with 4% PFA at 4 °C for at least 48 h for flow cytometry. All 293T infection experiments with EBOV were performed in the BSL4 laboratory of the Friedrich-Loeffler-Institute following approved standard operating procedures. MDM infection experiments were performed in the BSL4 laboratory of the Bernhard Nocht Institute for Tropical Medicine (BNITM) following approved standard operating procedures. Blood samples for MDM generation from eight donors were obtained from a cohort of healthy volunteers at the BNITM in Hamburg (Germany) with approved consent. The protocol for the use of these samples was authorized by the ethics committee of the German Medical Association and the ethics committee of the Ärztekammer Hamburg (PV4780).

Measles-virus (MeV) infection

293T control, CD81 KO, and HeLa cells were seeded in a 12-well plate format at a density of 1.5×10^5 (293T) or 3×10^5 (HeLa) cells per well. The following day they were infected with MeV-GFP (kindly provided by Ulrich Lauer, Virotherapy Center, Tübingen) diluted in Opti-MEM at an MOI of 0.1 or 1. A medium change was performed 3 h.p.i. and the cells were incubated for another 48 h at 37 °C. The infected cells were harvested, fixed with 2% PFA for 15 min at 37 °C, washed with PBS and measured using the flow

 © The Author(s)

cytometer. For tetraspanin modulation, cells were stained with PE-conjugated antibodies against CD81, CD63, and CD9. In order to assess the effect of CD81 (5A6) antibody treatment, cells were treated 1 h prior to infection with 1 μg/ml anti-human CD81 Antibody (5A6) or Mouse IgG1, κ Isotype Ctrl Antibody or left untreated.

Interaction prediction

The possible interaction between an EBOV GP trimer and CD81 was predicted using AlphaFold Server, powered by AlphaFold 3 (Abramson et al, 2024). EBOV GP (Q05320) and CD81 (P60033) amino acid sequences were retrieved from UniProtKB. The predicted model was then visualized with UCSF ChimeraX (Meng et al, 2023).

Software and analysis tools

FlowLogic (Inivai) and FlowJoc.10 was used for flow cytometry data analysis. Image Studio (LI-COR) was used for WB signals quantification. Incucyte (Sartorius) was used for quantification of microcopy images. ImageJ was used for IB, PLA, colocalization and p65 quantification of immunofluorescence microscopy images. Microsoft Excel and Graphpad Prism 9.4.1 were used for statistical analysis and Corel Draw for generation of figures.

Data availability

All data generated and analyzed during this study are included in this published manuscript. Our study includes no data deposited in public repositories.

The source data of this paper are collected in the following database record: biostudies:S-SCDT-10_1038-S44318-026-00940-8.

Expanded view data, supplementary information, appendices are available for this paper at https://doi.org/10.1038/s44318-026-00940-8.

Peer review information

A peer review file is available at https://doi.org/10.1038/s44318-026-00940-8

References

Abramson J, Adler J, Dunger J, Evans R, Green T, Pritzel A, Ronneberger O, Willmore L, Ballard AJ, Bambrick J et al (2024) Accurate structure prediction of biomolecular interactions with AlphaFold 3. Nature 630:493–500

Aleksandrowicz P, Marzi A, Biedenkopf N, Beimforde N, Becker S, Hoenen T, Feldmann H, Schnittler H-J (2011) Ebola virus enters host cells by macropinocytosis and clathrin-mediated endocytosis. J Infect Dis 204:S957–S967

Alvarez CP, Lasala F, Carrillo J, Muñiz O, Corbí AL, Delgado R (2002) C-type lectins DC-SIGN and L-SIGN mediate cellular entry by Ebola virus in cis and in trans. J Virol 76:6841–6844

Anand LK, Djurkovic MA, Shepley-McTaggart A, Shtanko O, Harty RN (2026) Tetraspanin CD9 Is a positive regulator of filovirus egress. Viruses 18:104

Andreu Z, Yanez-Mo M (2014) Tetraspanins in extracellular vesicle formation and function. Front Immunol 5:442

Baize S, Leroy EM, Georges AJ, Georges-Courbot MC, Capron M, Bedjabaga I, Lansoud-Soukate J, Mavoungou E (2002) Inflammatory responses in Ebola virus-infected patients. Clin Exp Immunol 128:163–168

Banan A, Zhang LJ, Shaikh M, Fields JZ, Farhadi A, Keshavarzian A (2004) Novel effect of NF-kappaB activation: carbonylation and nitration injury to cytoskeleton and disruption of monolayer barrier in intestinal epithelium. Am J Physiol Cell Physiol 287:C1139–1151

Banning C, Votteler J, Hoffmann D, Koppensteiner H, Warmer M, Reimer R, Kirchhoff F, Schubert U, Hauber J, Schindler M (2010) A flow cytometry-based FRET assay to identify and analyse protein-protein interactions in living cells. PLoS ONE 5:e9344

Bartosch B, Vitelli A, Granier C, Goujon C, Dubuisson J, Pascale S, Scarselli E, Cortese R, Nicosia A, Cosset F-L (2003) Cell entry of hepatitis C virus requires a set of co-receptors that include the CD81 tetraspanin and the SR-B1 scavenger receptor. J Biol Chem 278:41624–41630

Basler CF (2017) Molecular pathogenesis of viral hemorrhagic fever. Semin Immunopathol 39:551–561

Banse P, Moeller R, Bruening J, Lasswitz L, Kahl S, Khan AG, Marcotrigiano J, Pietschmann T, Gerold G (2018) CD81 Receptor Regions outside the Large Extracellular Loop Determine Hepatitis C Virus Entry into Hepatoma Cells. Viruses 10:207

Basler CF, Mikulasova A, Martinez-Sobrido L, Paragas J, Muhlberger E, Bray M, Klenk HD, Palese P, Garcia-Sastre A (2003) The Ebola virus VP35 protein inhibits activation of interferon regulatory factor 3. J Virol 77:7945–7956

Benayas B, Sastre I, Lopez-Martin S, Oo A, Kim B, Bullido MJ, Aldudo J, Yanez-Mo M (2020) Tetraspanin CD81 regulates HSV-1 infection. Med Microbiol Immunol 209:489–498

Beniac DR, Melito PL, deVarennes SL, Hiebert SL, Rabb MJ, Lamboo LL, Jones SM, Booth TF (2012) The organisation of Ebola virus reveals a capacity for extensive, modular polyploidy. PLoS ONE 7:e29608

Berditchevski F, Odintsova E (2007) Tetraspanins as regulators of protein trafficking. Traffic 8:89–96

Bharat TAM, Noda T, Riches JD, Kraehling V, Kolesnikova L, Becker S, Kawaoka Y, Briggs JAG (2012) Structural dissection of Ebola virus and its assembly determinants using cryo-electron tomography. Proc Natl Acad Sci USA 109:4275–4280

Bodmer BS, Vallbracht M, Ushakov DS, Wendt L, Chlanda P, Hoenen T (2023) Ebola virus inclusion bodies are liquid organelles whose formation is facilitated by nucleoprotein oligomerization. Emerg Microb Infect 12:2223727

Boutin M, Medjahed H, Nayrac M, Lotke R, Gendron-Lepage G, Bourassa C, Sauter D, Richard J, Finzi A (2023) Temsavir Modulates HIV-1 Envelope Conformation by Decreasing Its Proteolytic Cleavage. Viruses 15:1189

Braun E, Hotter D, Koepke L, Zech F, Groß R, Sparrer KMJ, Müller JA, Pfaller CK, Heusinger E, Wombacher R, Sutter K, Dittmer U, Winkler M, Simmons G, Jakobsen MR, Conzelmann KK, Pöhlmann S, Münch J, Fackler OT, Kirchhoff F, Sauter D (2019) Guanylate-Binding Proteins 2 and 5 Exert Broad Antiviral Activity by Inhibiting Furin-Mediated Processing of Viral Envelope Proteins. Cell Rep 27:2092-2104.e10

Brudner M, Karpel M, Lear C, Chen L, Yantosca LM, Scully C, Sarraju A, Sokolovska A, Zariffard MR, Eisen DP et al (2013) Lectin-dependent enhancement of ebola virus infection via soluble and transmembrane C-type lectin receptors. PLoS ONE 8:e60838

Bunz M, Eisele M, Hu D, Ritter M, Kammerloher J, Lampl S, Schindler M (2024) CD81 suppresses NF-kappaB signaling and is downregulated in hepatitis C virus expressing cells. Front Cell Infect Microbiol 14:1338606

© The Author(s)

Businger R, Deutschmann J, Gruska I, Milbradt J, Wiebusch L, Gramberg T, Schindler M. Human cytomegalovirus overcomes SAMHD1 restriction in macrophages via pUL97. Nat Microbiol. 2019;4:2260-2272.

Businger R, Kivimäki S, Simeonov S, Vavouras Syrigos G, Pohlmann J, Bolz M, Müller P, Codrea MC, Templin C, Messerle M et al (2021) Comprehensive analysis of human cytomegalovirus- and HIV-mediated plasma membrane remodeling in macrophages. mBio 12:e0177021. 10.1128/mbio.01770–01721

Cardenas WB, Loo YM, Gale M Jr, Hartman AL, Kimberlin CR, Martinez-Sobrido L, Saphire EO, Basler CF (2006) Ebola virus VP35 protein binds double-stranded RNA and inhibits alpha/beta interferon production induced by RIG-I signaling. J Virol 80:5168–5178

Chandran K, Sullivan NJ, Felbor U, Whelan SP, Cunningham JM (2005) Endosomal proteolysis of the Ebola virus glycoprotein is necessary for infection. Science 308:1643–1645

Chang GW, Hsiao CC, Peng YM, Vieira Braga FA, Kragten NA, Remmerswaal EB, van de Garde MD, Straussberg R, König GM, Kostenis E, Knäuper V, Meyaard L, van Lier RA, van Gisbergen KP, Lin HH, Hamann J (2016) The Adhesion G Protein-Coupled Receptor GPR56/ADGRG1 Is an Inhibitory Receptor on Human NK Cells. Cell Rep 15:1757-70

Chang TH, Kubota T, Matsuoka M, Jones S, Bradfute SB, Bray M, Ozato K (2009) Ebola Zaire virus blocks type I interferon production by exploiting the host SUMO modification machinery. PLoS Pathog 5:e1000493

Charrin S, Jouannet S, Boucheix C, Rubinstein E (2014) Tetraspanins at a glance. J Cell Sci 127:3641–3648

Chen J, He Z, Yuan Y, Huang F, Luo B, Zhang J, Pan T, Zhang H, Zhang J (2019) Host factor SMYD3 is recruited by Ebola virus nucleoprotein to facilitate viral mRNA transcription. Emerg Microb Infect 8:1347–1360

Chiasson-MacKenzie C, Morris ZS, Liu C-H, Bradford WB, Koorman T, McClatchey AI (2018) Merlin/ERM proteins regulate growth factor-induced macropinocytosis and receptor recycling by organizing the plasma membrane:cytoskeleton interface. Genes Dev 32:1201–1214

Côté M, Misasi J, Ren T, Bruchez A, Lee K, Filone CM, Hensley L, Li Q, Ory D, Chandran K et al (2011) Small molecule inhibitors reveal Niemann–Pick C1 is essential for Ebola virus infection. Nature 477:344–348

Deneka M, Pelchen-Matthews A, Byland R, Ruiz-Mateos E, Marsh M (2007) In macrophages, HIV-1 assembles into an intracellular plasma membrane domain containing the tetraspanins CD81, CD9, and CD53. J Cell Biol 177:329–341

Dolnik O, Gerresheim GK, Biedenkopf N (2021) New perspectives on the biogenesis of viral inclusion bodies in negative-sense RNA virus infections. Cells 10:1460

Domanico SZ, Pelletier AJ, Havran WL, Quaranta V (1997) Integrin alpha 6 A beta 1 induces CD81-dependent cell motility without engaging the extracellular matrix migration substrate. Mol Biol Cell 8:2253–2265

Elliott LH, Kiley MP, McCormick JB (1985) Descriptive analysis of Ebola virus proteins. Virology 147:169–176

Escudero-Perez B, Volchkova VA, Dolnik O, Lawrence P, Volchkov VE (2014) Shed GP of Ebola virus triggers immune activation and increased vascular permeability. PLoS Pathog 10:e1004509

Feldmann H, Geisbert TW (2011) Ebola haemorrhagic fever. Lancet 377:849–862

Florin L, Lang T (2018) Tetraspanin assemblies in virus infection. Front Immunol 9:1140

Francica JR, Varela-Rohena A, Medvec A, Plesa G, Riley JL, Bates P (2010) Steric shielding of surface epitopes and impaired immune recognition induced by the Ebola virus glycoprotein. PLoS Pathog 6:e1001098

Fujii M, Kawai K, Egami Y, Araki N (2013) Dissecting the roles of Rac1 activation and deactivation in macropinocytosis using microscopic photo-manipulation. Sci Rep 3:2385

Gramberg T, Kahle T, Bloch N, Wittmann S, Müllers E, Daddacha W, Hofmann H, Kim B, Lindemann D, Landau NR (2013) Restriction of diverse retroviruses by SAMHD1. Retrovirology 10:26

Gräßel L, Fast LA, Scheffer KD, Boukhallouk F, Spoden GA, Tenzer S, Boller K, Bago R, Rajesh S, Overduin M et al (2016) The CD63-syntenin-1 complex controls post-endocytic trafficking of oncogenic human papillomaviruses. Sci Rep 6:32337

Groseth A, Charton JE, Sauerborn M, Feldmann F, Jones SM, Hoenen T, Feldmann H (2009) The Ebola virus ribonucleoprotein complex: a novel VP30–L interaction identified. Virus Res 140:8–14

Hagelauer E, Lotke R, Kmiec D, Hu D, Hohner M, Stopper S, Nchioua R, Kirchhoff F, Sauter D, Schindler M (2023) Tetherin Restricts SARS-CoV-2 despite the Presence of Multiple Viral Antagonists. Viruses 15:2364

Hanke K, Kramer P, Seeher S, Beimforde N, Kurth R, Bannert N (2009) Reconstitution of the ancestral glycoprotein of human endogenous retrovirus k and modulation of its functional activity by truncation of the cytoplasmic domain. J Virol 83:12790-800

Harcourt BH, Sanchez A, Offermann MK (1999) Ebola virus selectively inhibits responses to interferons, but not to interleukin-1beta, in endothelial cells. J Virol 73:3491–3496

Heumos S, Dehn S, Bräutigam K, Codrea MC, Schürch CM, Lauer UM, Nahnsen S, Schindler M (2022) Multiomics surface receptor profiling of the NCI-60 tumor cell panel uncovers novel theranostics for cancer immunotherapy. Cancer Cell Int 22:311

Hoenen T, Groseth A, Callison J, Takada A, Feldmann H (2013) A novel Ebola virus expressing luciferase allows for rapid and quantitative testing of antivirals. Antiviral Res 99:207–213

Hoenen T, Shabman RS, Groseth A, Herwig A, Weber M, Schudt G, Dolnik O, Basler CF, Becker S, Feldmann H (2012) Inclusion bodies are a site of ebolavirus replication. J Virol 86:11779–11788

Horvath G, Serru V, Clay D, Billard M, Boucheix C, Rubinstein E (1998) CD19 is linked to the integrin-associated tetraspans CD9, CD81, and CD82. J Biol Chem 273:30537–30543

Huang Y, Xu L, Sun Y, Nabel GJ (2002) The assembly of Ebola virus nucleocapsid requires virion-associated proteins 35 and 24 and posttranslational modification of nucleoprotein. Mol Cell 10:307–316

Hume AJ, Mühlberger E (2019) Distinct genome replication and transcription strategies within the growing filovirus family. J Mol Biol 431:4290–4320

Iraqi M, Edri A, Greenshpan Y, Kundu K, Bolel P, Cahana A, Ottolenghi A, Gazit R, Lobel L, Braiman A et al (2020) N-glycans mediate the Ebola virus-GP1 shielding of ligands to immune receptors and immune evasion. Front Cell Infect Microbiol 10:48

Jasenosky LD, Neumann G, Lukashevich I, Kawaoka Y (2001) Ebola virus VP40-induced particle formation and association with the lipid bilayer. J Virol 75:5205–5214

Jemielity S, Wang JJ, Chan YK, Ahmed AA, Li W, Monahan S, Bu X, Farzan M, Freeman GJ, Umetsu DT et al (2013) TIM-family proteins promote infection of multiple enveloped viruses through virion-associated phosphatidylserine. PLoS Pathog 9:e1003232

Jolly C, Sattentau QJ (2007) Human immunodeficiency virus type 1 assembly, budding, and cell-cell spread in T cells take place in tetraspanin-enriched plasma membrane domains. J Virol 81:7873–7884

Kaletsky RL, Francica JR, Agrawal-Gamse C, Bates P (2009) Tetherin-mediated restriction of filovirus budding is antagonized by the Ebola glycoprotein. Proc Natl Acad Sci USA 106:2886–2891

Kay RR (2021) Macropinocytosis: biology and mechanisms. Cells Dev 168:203713

Kirchdoerfer Robert N, Abelson Dafna M, Li S, Wood Malcolm R, Saphire Erica O (2015) Assembly of the Ebola virus nucleoprotein from a chaperoned VP35 complex. Cell Rep 12:140–149

 © The Author(s)

Kondratowicz AS, Lennemann NJ, Sinn PL, Davey RA, Hunt CL, Moller-Tank S, Meyerholz DK, Rennert P, Mullins RF, Brindley M et al (2011) T-cell immunoglobulin and mucin domain 1 (TIM-1) is a receptor for Zaire Ebolavirus and Lake Victoria Marburgvirus. Proc Natl Acad Sci USA 108:8426–8431

Koppensteiner H, Banning C, Schneider C, Hohenberg H, Schindler M (2012) Macrophage internal HIV-1 is protected from neutralizing antibodies. J Virol 86:2826–2836

Krollmann C, Cieslak K, Koerber R-M, Luksch H, Rösen-Wolff A, Brossart P, Teichmann LL (2022) Quantification of unperturbed phosphoprotein levels in immune cell subsets with phosphoflow to assess immune signaling in autoimmune disease. STAR Protoc 3:101309

Kuhl A, Banning C, Marzi A, Votteler J, Steffen I, Bertram S, Glowacka I, Konrad A, Sturzl M, Guo JT et al (2011) The Ebola virus glycoprotein and HIV-1 Vpu employ different strategies to counteract the antiviral factor tetherin. J Infect Dis 204:S850–860

Kuhn JH, Adachi T, Adhikari NKJ, Arribas JR, Bah IE, Bausch DG, Bhadelia N, Borchert M, Brantsæter AB, Brett-Major DM et al (2019a) New filovirus disease classification and nomenclature. Nat Rev Microbiol 17:261–263

Kuhn JH, Amarasinghe GK, Basler CF, Bavari S, Bukreyev A, Chandran K, Crozier I, Dolnik O, Dye JM, Formenty PBH et al (2019b) ICTV virus taxonomy profile: *Filoviridae*. J Gen Virol 100:911–912

Lambele M, Koppensteiner H, Symeonides M, Roy NH, Chan J, Schindler M, Thali M (2015) Vpu is the main determinant for tetraspanin downregulation in HIV-1-infected cells. J Virol 89:3247–3255

Lasswitz L, Zapatero-Belinchon FJ, Moeller R, Hulskotter K, Laurent T, Carlson LA, Goffinet C, Simmons G, Baumgartner W, Gerold G (2022) The tetraspanin CD81 is a host factor for chikungunya virus replication. mBio 13:e0073122

Leung Daisy W, Borek D, Luthra P, Binning Jennifer M, Anantpadma M, Liu G, Harvey Ian B, Su Z, Endlich-Frazier A, Pan J et al (2015) An intrinsically disordered peptide from Ebola virus VP35 controls viral RNA synthesis by modulating nucleoprotein-RNA interactions. Cell Rep 11:376–389

Levy S, Shoham T (2005) The tetraspanin web modulates immune-signalling complexes. Nat Rev Immunol 5:136–148

Licata JM, Johnson RF, Han Z, Harty RN (2004) Contribution of Ebola virus glycoprotein, nucleoprotein, and VP24 to budding of VP40 virus-like particles. J Virol 78:7344–7351

Lier C, Becker S, Biedenkopf N (2017) Dynamic phosphorylation of Ebola virus VP30 in NP-induced inclusion bodies. Virology 512:39–47

Lim J, Petersen M, Bunz M, Simon C, Schindler M (2022) Flow cytometry based-FRET: basics, novel developments and future perspectives. Cell Mol Life Sci 79:217

Luo JL, Kamata H, Karin M (2005) IKK/NF-kappaB signaling: balancing life and death-a new approach to cancer therapy. J Clin Invest 115:2625–2632

Maecker HT, Todd SC, Levy S (1997) The tetraspanin superfamily: molecular facilitators. FASEB J 11:428–442

Maminska A, Bartosik A, Banach-Orlowska M, Pilecka I, Jastrzebski K, Zdzalik-Bielecka D, Castanon I, Poulain M, Neyen C, Wolinska-Niziol L et al (2016) ESCRT proteins restrict constitutive NF-kappaB signaling by trafficking cytokine receptors. Sci Signal 9:ra8

Martínez MJ, Biedenkopf N, Volchkova V, Hartlieb B, Alazard-Dany N, Reynard O, Becker S, Volchkov V (2008) Role of Ebola virus VP30 in transcription reinitiation. J Virol 82:12569–12573

Martins SA, Correia PD, Dias RA, da Cruz ESOAB, Vieira SI (2019) CD81 promotes a migratory phenotype in neuronal-like cells. Microsc Microanal 25:229–235

Mehedi M, Falzarano D, Seebach J, Hu X, Carpenter MS, Schnittler H-J, Feldmann H (2011) A new Ebola virus nonstructural glycoprotein expressed through RNA editing. J Virol 85:5406–5414

Meng EC, Goddard TD, Pettersen EF, Couch GS, Pearson ZJ, Morris JH, Ferrin TE (2023) UCSF ChimeraX: Tools for structure building and analysis. Protein Sci 32:e4792

Mikuličić S, Fritzen A, Scheffer K, Strunk J, Cabañas C, Sperrhacke M, Reiss K, Florin L (2020) Tetraspanin CD9 affects HPV16 infection by modulating ADAM17 activity and the ERK signalling pathway. Med Microbiol Immunol 209:461–471

Miyake T, Farley CM, Neubauer BE, Beddow TP, Hoenen T, Engel DA (2020) Ebola virus inclusion body formation and RNA synthesis are controlled by a novel domain of nucleoprotein interacting with VP35. J Virol 94:e02100–02119

Moller-Tank S, Maury W (2015) Ebola virus entry: a curious and complex series of events. PLoS Pathog 11:e1004731

Mühlberger E, Weik M, Volchkov VE, Klenk H-D, Becker S (1999) Comparison of the transcription and replication strategies of Marburg virus and ebola virus by using artificial replication systems. J Virol 73:2333–2342

Nanbo A, Imai M, Watanabe S, Noda T, Takahashi K, Neumann G, Halfmann P, Kawaoka Y (2010) Ebolavirus is internalized into host cells via macropinocytosis in a viral glycoprotein-dependent manner. PLoS Pathog 6:e1001121

Nanbo A, Watanabe S, Halfmann P, Kawaoka Y (2013) The spatio-temporal distribution dynamics of Ebola virus proteins and RNA in infected cells. Sci Rep 3:1206

Nehls J, Businger R, Hoffmann M, Brinkmann C, Fehrenbacher B, Schaller M, Maurer B, Schönfeld C, Kramer D, Hailfinger S et al (2019) Release of immunomodulatory Ebola virus glycoprotein-containing microvesicles is suppressed by tetherin in a species-specific manner. Cell Rep 26:1841–1853.e1846

Nemeth ZH, Deitch EA, Davidson MT, Szabo C, Vizi ES, Hasko G (2004) Disruption of the actin cytoskeleton results in nuclear factor-kappaB activation and inflammatory mediator production in cultured human intestinal epithelial cells. J Cell Physiol 200:71–81

Nydegger S, Khurana S, Krementsov DN, Foti M, Thali M (2006) Mapping of tetraspanin-enriched microdomains that can function as gateways for HIV-1. J Cell Biol 173:795–807

Oeckinghaus A, Ghosh S (2009) The NF-kappaB family of transcription factors and its regulation. Cold Spring Harb Perspect Biol 1:a000034

Oguri Y, Shinoda K, Kim H, Alba DL, Bolus WR, Wang Q, Brown Z, Pradhan RN, Tajima K, Yoneshiro T et al (2020) CD81 controls beige fat progenitor cell growth and energy balance via FAK signaling. Cell 182:563–577.e520

Okumura A, Pitha PM, Yoshimura A, Harty RN (2010) Interaction between Ebola virus glycoprotein and host toll-like receptor 4 leads to induction of proinflammatory cytokines and SOCS1. J Virol 84:27–33

Oren R, Takahashi S, Doss C, Levy R, Levy S (1990) TAPA-1, the target of an antiproliferative antibody, defines a new family of transmembrane proteins. Mol Cell Biol 10:4007–4015

Peng W, Rayaprolu V, Parvate AD, Pronker MF, Hui S, Parekh D, Shaffer K, Yu X, Saphire EO, Snijder J (2022) Glycan shield of the ebolavirus envelope glycoprotein GP. Commun Biol 5:785

Pfaffl MW (2001) A new mathematical model for relative quantification in real-time RT–PCR. Nucleic Acids Res 29:e45

Pham TN, Richard J, Gerard FC, Power C, Cohen ÉA (2011) Modulation of NKG2D-mediated cytotoxic functions of natural killer cells by viral protein R from HIV-1 primary isolates. J Virol 85:12254-61. https://doi.org/10.1128/JVI.05835-11. Erratum in: (2012) J Virol. 86:1902

Powlesland AS, Fisch T, Taylor ME, Smith DF, Tissot B, Dell A, Pöhlmann S, Drickamer K (2008) A novel mechanism for LSECtin binding to Ebola virus surface glycoprotein through truncated glycans. J Biol Chem 283:593–602

Ramos EK, Tsai CF, Jia Y, Cao Y, Manu M, Taftaf R, Hoffmann AD, El-Shennawy L, Gritsenko MA, Adorno-Cruz V et al (2022) Machine learning-assisted

© The Author(s)

elucidation of CD81-CD44 interactions in promoting cancer stemness and extracellular vesicle integrity. Elife 11:e82669

Reppert N, Lang T (2022) A conserved sequence in the small intracellular loop of tetraspanins forms an M-shaped inter-helix turn. Sci Rep 12:4494

Reynard O, Borowiak M, Volchkova VA, Delpeut S, Mateo M, Volchkov VE (2009) Ebolavirus glycoprotein GP masks both its own epitopes and the presence of cellular surface proteins. J Virol 83:9596–9601

Reynard S, Journeaux A, Gloaguen E, Schaeffer J, Varet H, Pietrosemoli N, Mateo M, Baillet N, Laouenan C, Raoul H et al (2019) Immune parameters and outcomes during Ebola virus disease. JCI Insight 4:e125106

Rizk MG, Basler CF, Guatelli J (2017) Cooperation of the Ebola virus proteins VP40 and GP(1,2) with BST2 To activate NF-kappaB independently of virus-like particle trapping. J Virol 91:e01308–17

Saeed MF, Kolokoltsov AA, Albrecht T, Davey RA (2010) Cellular entry of Ebola virus involves uptake by a macropinocytosis-like mechanism and subsequent trafficking through early and late endosomes. PLoS Pathog 6:e1001110

Sala-Valdés M, Ursa Á, Charrin S, Rubinstein E, Hemler ME, Sánchez-Madrid F, Yáñez-Mó M (2006) EWI-2 and EWI-F link the tetraspanin web to the actin cytoskeleton through their direct association with Ezrin-Radixin-Moesin proteins. J Biol Chem 281:19665–19675

Salditt A, Koethe S, Pohl C, Harms H, Kolesnikova L, Becker S, Schneider-Schaulies S (2010) Measles virus M protein-driven particle production does not involve the endosomal sorting complex required for transport (ESCRT) system. J Gen Virol 91:1464–1472

Sanchez A, Kiley MP, Holloway BP, Auperin DD (1993) Sequence analysis of the Ebola virus genome: organization, genetic elements, and comparison with the genome of Marburg virus. Virus Res 29:215–240

Sanchez A, Trappier SG, Mahy BW, Peters CJ, Nichol ST (1996) The virion glycoproteins of Ebola viruses are encoded in two reading frames and are expressed through transcriptional editing. Proc Natl Acad Sci USA 93:3602–3607

Sauter D, Hué S, Petit SJ, Plantier JC, Towers GJ, Kirchhoff F, Gupta RK (2011) HIV-1 Group P is unable to antagonize human tetherin by Vpu, Env or Nef. Retrovirology 8:103

Scheffer KD, Gawlitza A, Spoden GA, Zhang XA, Lambert C, Berditchevski F, Florin L (2013) Tetraspanin CD151 mediates papillomavirus type 16 endocytosis. J Virol 87:3435–3446

Scherm MJ, Gangloff M, Gay NJ (2022) Activation of Toll-like receptor 4 by Ebola virus-shed glycoprotein is direct and requires the internal fusion loop but not glycosylation. Cell Rep 41:111562

Schindler M, Würfl S, Benaroch P, Greenough TC, Daniels R, Easterbrook P, Brenner M, Münch J, Kirchhoff F (2023) Down-modulation of mature major histocompatibility complex class II and up-regulation of invariant chain cell surface expression are well-conserved functions of human and simian immunodeficiency virus nef alleles. J Virol 77:10548-56

Schmidt ML, Tews BA, Groseth A, Hoenen T (2018) Generation and optimization of a green fluorescent protein-expressing transcription and replication-competent virus-like particle system for ebola virus. J Infect Dis 218:S360–S364

Schornberg K, Matsuyama S, Kabsch K, Delos S, Bouton A, White J (2006) Role of endosomal cathepsins in entry mediated by the ebola virus glycoprotein. J Virol 80:4174–4178

Schornberg KL, Shoemaker CJ, Dube D, Abshire MY, Delos SE, Bouton AH, White JM (2009) α5β1-Integrin controls ebolavirus entry by regulating endosomal cathepsins. Proc Natl Acad Sci USA 106:8003–8008

Serru V, Le Naour F, Billard M, Azorsa DO, Lanza F, Boucheix C, Rubinstein E (1999) Selective tetraspan-integrin complexes (CD81/alpha4beta1, CD151/alpha3beta1, CD151/alpha6beta1) under conditions disrupting tetraspan interactions. Biochem J 340:103–111

Shabman RS, Hoenen T, Groseth A, Jabado O, Binning JM, Amarasinghe GK, Feldmann H, Basler CF (2013) An upstream open reading frame modulates ebola virus polymerase translation and virus replication. PLoS Pathog 9:e1003147

Sharma S, tenOever BR, Grandvaux N, Zhou GP, Lin R, Hiscott J (2003) Triggering the interferon antiviral response through an IKK-related pathway. Science 300:1148–1151

Shimojima M, Takada A, Ebihara H, Neumann G, Fujioka K, Irimura T, Jones S, Feldmann H, Kawaoka Y (2006) Tyro3 family-mediated cell entry of Ebola and Marburg viruses. J Virol 80:10109–10116

Simmons G, Wool-Lewis RJ, Baribaud F, Netter RC, Bates P (2002) Ebola virus glycoproteins induce global surface protein down-modulation and loss of cell adherence. J Virol 76:2518–2528

Spence JS, Krause TB, Mittler E, Jangra RK, Chandran K (2016) Direct visualization of ebola virus fusion triggering in the endocytic pathway. mBio 7:e01857–01815

Suffner S, Gerstenberg N, Patra M, Ruibal P, Orabi A, Schindler M, Bruss V (2018) Domains of the Hepatitis B Virus Small Surface Protein S Mediating Oligomerization. J Virol 92:e02232-17

Sullivan NJ, Peterson M, Yang Z-Y, Kong W-P, Duckers H, Nabel E, Nabel GJ (2005) Ebola virus glycoprotein toxicity is mediated by a dynamin-dependent protein-trafficking pathway. J Virol 79:547–553

Susa KJ, Seegar TCM, Blacklow SC, Kruse AC (2020) A dynamic interaction between CD19 and the tetraspanin CD81 controls B cell co-receptor trafficking. eLife 9:e52337

Takada A, Fujioka K, Tsuiji M, Morikawa A, Higashi N, Ebihara H, Kobasa D, Feldmann H, Irimura T, Kawaoka Y (2004) Human macrophage C-type lectin specific for galactose and N -acetylgalactosamine promotes filovirus entry. J Virol 78:2943–2947

Takamatsu Y, Yoshikawa T, Kurosu T, Fukushi S, Nagata N, Shimojima M, Ebihara H, Saijo M, Noda T (2022) Role of VP30 phosphorylation in Ebola virus nucleocapsid assembly and transport. J Virol 96:e01083–01022

Tejera E, Rocha-Perugini V, López-Martín S, Pérez-Hernández D, Bachir AI, Horwitz AR, Vázquez J, Sánchez-Madrid F, Yáñez-Mo M (2013) CD81 regulates cell migration through its association with Rac GTPase. Mol Biol Cell 24:261–273

Termini CM, Gillette JM (2017) Tetraspanins function as regulators of cellular signaling. Front Cell Dev Biol 5:34

Umeda R, Satouh Y, Takemoto M, Nakada-Nakura Y, Liu K, Yokoyama T, Shirouzu M, Iwata S, Nomura N, Sato K et al (2020) Structural insights into tetraspanin CD9 function. Nat Commun 11:1606

Vences-Catalán F, Kuo C-C, Rajapaksa R, Duault C, Andor N, Czerwinski DK, Levy R, Levy S (2019) CD81 is a novel immunotherapeutic target for B cell lymphoma. J Exp Med 216:1497–1508

Vences-Catalán F, Rajapaksa R, Kuo C-C, Miller CL, Lee A, Ramani VC, Jeffrey SS, Levy R, Levy S (2021) Targeting the tetraspanin CD81 reduces cancer invasion and metastasis. Proc Natl Acad Sci USA 118:e2018961118

Verzella D, Pescatore A, Capece D, Vecchiotti D, Ursini MV, Franzoso G, Alesse E, Zazzeroni F (2020) Life, death, and autophagy in cancer: NF-kappaB turns up everywhere. Cell Death Dis 11:210

Volchkov VE, Becker S, Volchkova VA, Ternovoj VA, Kotov AN, Netesov SV, Klenk H-D (1995) GP mRNA of Ebola virus is edited by the Ebola virus polymerase and by T7 and vaccinia virus polymerases. Virology 214:421–430

Volchkov VE, Volchkova VA, Slenczka W, Klenk H-D, Feldmann H (1998) Release of viral glycoproteins during Ebola virus infection. Virology 245:110–119

Watt A, Moukambi F, Banadyga L, Groseth A, Callison J, Herwig A, Ebihara H, Feldmann H, Hoenen T (2014) A novel life cycle modeling system for ebola virus shows a genome length-dependent role of VP24 in virus infectivity. J Virol 88:10511–10524

 © The Author(s)

Weik M, Modrof J, Klenk H-D, Becker S, Mühlberger E (2002) Ebola virus VP30-mediated transcription is regulated by RNA secondary structure formation. J Virol 76:8532–8539

Wendt L, Brandt J, Bodmer BS, Reiche S, Schmidt ML, Traeger S, Hoenen T (2020) The Ebola Virus Nucleoprotein Recruits the Nuclear RNA Export Factor NXF1 into Inclusion Bodies to Facilitate Viral Protein Expression. Cells 9:187

WHO (2023a) Ebola virus disease. https://www.who.int/news-room/fact-sheets/detail/ebola-virus-disease

WHO (2023b) Marburg virus disease. https://www.who.int/news-room/fact-sheets/detail/marburg-virus-disease

Wu C, Wagner ND, Moyle AB, Feng A, Sharma N, Stubbs SH, Donahue C, Davey RA, Gross ML, Leung DW et al (2023) Disruption of Ebola NP(0)VP35 inclusion body-like structures reduce viral infection. J Mol Biol 435:168241

Yamaoka S, M'Hamdi Z, Wang L, Swenson VA, McNally KL, Lu SC, Singh R, Saundh SL, Zell BN, Best SM et al (2026) Ebola virus matrix protein VP40 triggers inflammatory responses linked to the ebolavirus virulence. Proc Natl Acad Sci USA 123:e2508194123

Yáñez-Mó M, Barreiro O, Gordon-Alonso M, Sala-Valdés M, Sánchez-Madrid F (2009) Tetraspanin-enriched microdomains: a functional unit in cell plasma membranes. Trends Cell Biol 19:434–446

Yuan S, Cao L, Ling H, Dang M, Sun Y, Zhang X, Chen Y, Zhang L, Su D, Wang X et al (2015) TIM-1 acts a dual-attachment receptor for Ebolavirus by interacting directly with viral GP and the PS on the viral envelope. Protein Cell 6:814–824

Zampieri CA, Fortin J-F, Nolan GP, Nabel GJ (2007) The ERK mitogen-activated protein kinase pathway contributes to Ebola virus glycoprotein-induced cytotoxicity. J Virol 81:1230–1240

Zimmerman B, Kelly B, McMillan BJ, Seegar TCM, Dror RO, Kruse AC, Blacklow SC (2016) Crystal structure of a full-length human tetraspanin reveals a cholesterol-binding pocket. Cell 167:1041–1051.e1011

Acknowledgements

We thank Daniel Sauter (Tübingen), Thomas Gramberg (Erlangen), Johannes Schmidt (Wien), and Stefan Pöhlmann (Göttingen) for the kind contribution of cell lines, reagents and plasmids. Furthermore Ulrich Lauer (Tübingen) for support with MeV-GFP. Dan Hu received a PhD scholarship from the China Scholarship Council (CSC). This work was further supported by a DFG German Research Foundation grant to MS (SCHI 1073/10-1, project number 399732171), as well as basic research support from the University Hospital Tübingen, Medical Faculty to MS. We acknowledge support from the Open Access Publication Fund of the University of Tübingen.

Author contributions

Dan Hu: Conceptualization; Data curation; Formal analysis; Funding acquisition; Validation; Investigation; Visualization; Methodology; Writing—review and editing. **Elena Hagelauer**: Conceptualization; Data curation; Formal analysis; Validation; Investigation; Visualization; Methodology; Writing—review and editing. **Lisa Wendt**: Investigation; Methodology; Writing—review and editing. **Matteo Bosso**: Investigation; Methodology; Writing—review and editing. **Maximilian Bunz**: Investigation; Methodology; Writing—review and editing. **Julia Kammerloher**: Investigation; Writing—review and editing. **Jasmin Kutter**: Investigation; Writing—review and editing. **Johannes Brandi**: Data curation; Validation; Investigation; Methodology; Writing—review and editing. **Lina Widerspick**: Data curation; Validation; Investigation; Methodology; Writing—review and editing. **Thomas Hoenen**: Conceptualization; Resources; Supervision; Investigation; Writing—review and editing. **Michael Schindler**: Conceptualization; Resources; Data curation; Formal analysis; Supervision; Funding acquisition; Validation; Investigation; Visualization; Methodology; Writing—original draft; Project administration.

Source data underlying figure panels in this paper may have individual authorship assigned. Where available, figure panel/source data authorship is listed in the following database record: biostudies:S-SCDT-10_1038-S44318-026-00940-8.

Funding

Open Access funding enabled and organized by Projekt DEAL.

Disclosure and competing interests statement

The authors declare no competing interests.

Open Access This article is licensed under a Creative Commons Attribution 4.0 International License, which permits use, sharing, adaptation, distribution and reproduction in any medium or format, as long as you give appropriate credit to the original author(s) and the source, provide a link to the Creative Commons licence, and indicate if changes were made. The images or other third party material in this article are included in the article's Creative Commons licence, unless indicated otherwise in a credit line to the material. If material is not included in the article's Creative Commons licence and your intended use is not permitted by statutory regulation or exceeds the permitted use, you will need to obtain permission directly from the copyright holder. To view a copy of this licence, visit http://creativecommons.org/licenses/by/4.0/. Creative Commons Public Domain Dedication waiver http://creativecommons.org/publicdomain/zero/1.0/ applies to the data associated with this article, unless otherwise stated in a credit line to the data, but does not extend to the graphical or creative elements of illustrations, charts, or figures. This waiver removes legal barriers to the re-use and mining of research data. According to standard scholarly practice, it is recommended to provide appropriate citation and attribution whenever technically possible.

© The Author(s) 2026

Expanded View Figures

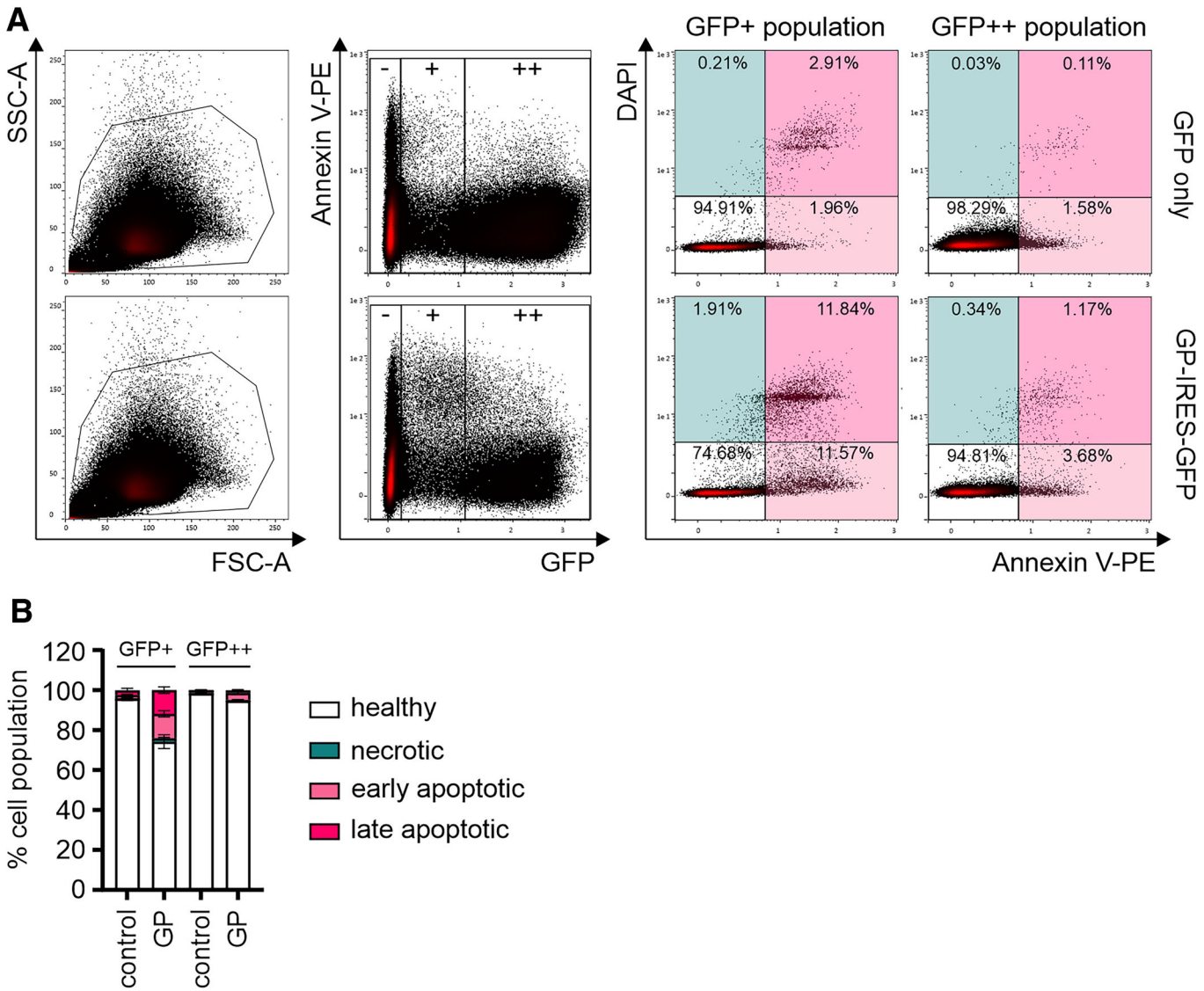
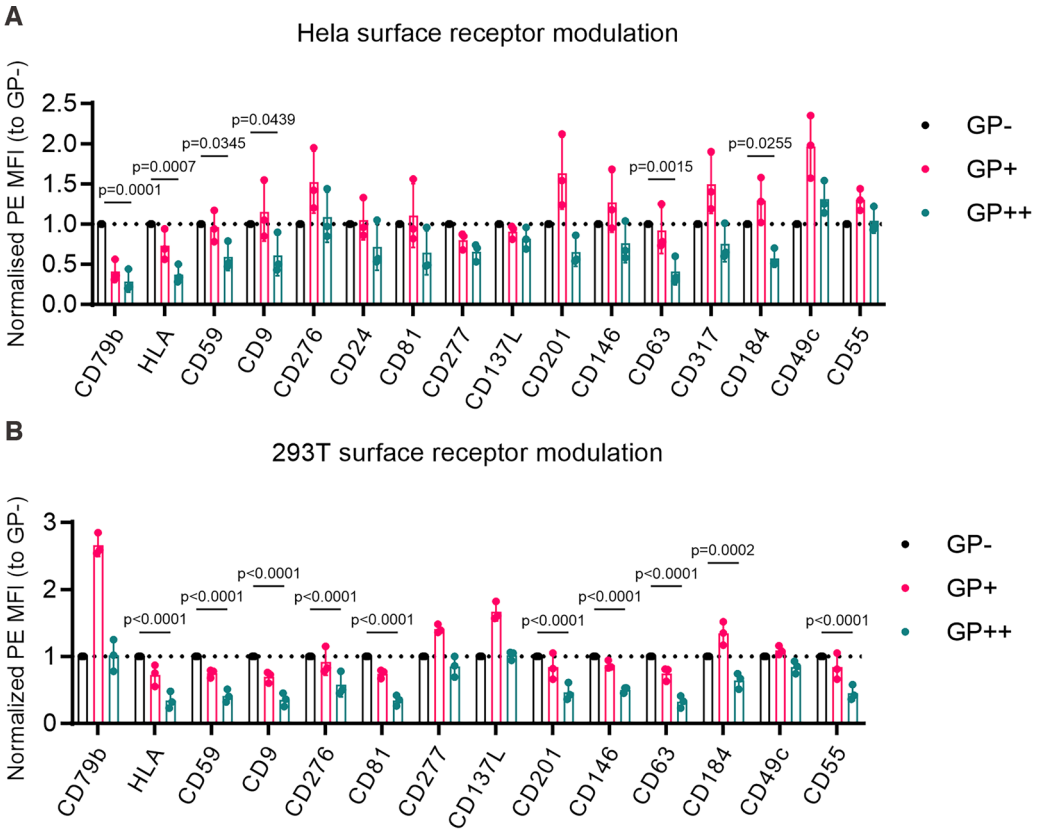
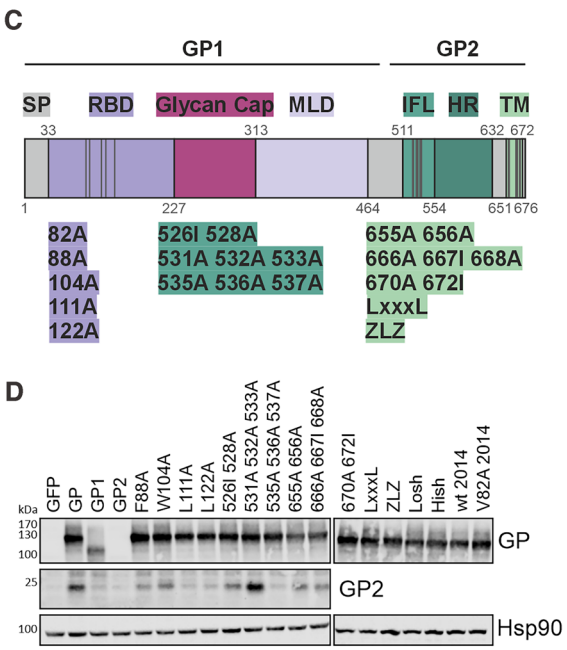


Figure EV1. Flow cytometry gating and EBOV GP-induced cytotoxicity.

(**A**) 293T cells were GFP-only transfected (top) or transfected to coexpress GFP and EBOV GP (bottom). The general population of living cells was gated according to SSC-A and FSC-A (left panel of density plots). 2 d.p.t., the cells were stained with Annexin V (AnV)-PE and DAPI to detect healthy (AnV-/DAPI-), necrotic (AnV-/DAPI+), early apoptotic (AnV+/DAPI−) or late apoptotic (AnV+/DAPI+) cells (right panel of density plots). We further included two regions of medium (+) or high (++) levels of GFP, hence GP-expression. (**B**) Quantification of the percentage of healthy, necrotic, early and late apoptotic cells in GFP-only control or GP-expressing 293T cells according to regions of medium (GFP+) or high (GFP+) levels of GFP/GP expression. The diagram shows stacked columns indicating the mean values of the relative percentage of the respective cell fraction ±SD of three independent experiments.

© The Author(s)


A
Hela surface receptor modulation
Normalised PE MFI (to GP-)
p=0.0001
p=0.0007
p=0.0345
p=0.0439
p=0.0015
p=0.0255
GP-
GP+
GP++
CD79b HLA CD59 CD9 CD276 CD24 CD81 CD277 CD137L CD201 CD146 CD63 CD317 CD184 CD49c CD55
B
293T surface receptor modulation
Normalized PE MFI (to GP-)
p<0.0001
p=0.0002
GP-
GP+
GP++
CD79b HLA CD59 CD9 CD276 CD81 CD277 CD137L CD201 CD146 CD63 CD184 CD49c CD55


C
GP1
GP2
SP RBD Glycan Cap MLD IFL HR TM
33 313 511 632 672
1 227 464 554 651 676
82A
88A
104A
111A
122A
526I 528A
531A 532A 533A
535A 536A 537A
655A 656A
666A 667I 668A
670A 672I
LxxxL
ZLZ
D
GFP GP GP1 GP2 F88A W104A L111A L122A 526I 528A 531A 532A 533A 535A 536A 537A 655A 656A 666A 667I 668A 670A 672I LxxxL ZLZ Losh Hish wt 2014 V82A 2014
kDa
170
130
100
25
100
GP
GP2
Hsp90

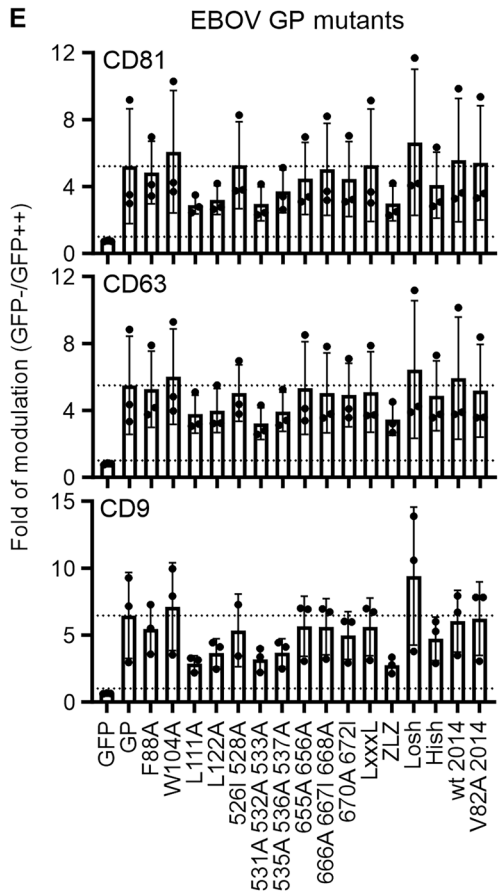

E
EBOV GP mutants
CD81
CD63
CD9
Fold of modulation (GFP-/GFP++)
GFP GP F88A W104A L111A L122A 526I 528A 531A 532A 533A 535A 536A 537A 655A 656A 666A 667I 668A 670A 672I LxxxL ZLZ Losh Hish wt 2014 V82A 2014

Figure EV2. Modulation of surface proteins by EBOV GP and GP mutants.

(**A**, **B**) Relative expression (PE MFI normalized to GP- cells) of surface proteins (twofold higher than unstained ctrl) in (**A**) HeLa and (**B**) 293T cells according to no (−), medium (+) and high (++) levels of GFP and hence GP expression (data related to Fig. 1B; Dataset EV2). Shown are mean values ± SD from $n = 3$ independent experiments. Two-way ANOVA with Dunnett correction was used for statistical analysis. (**C**) Scheme of EBOV GP domain structure with indicated mutations. Structural domains are highlighted in color: signal peptide (SP), receptor-binding-domain (RBD), mucin-like domain (MLD), internal fusion loop (IFL), heptad repeats (HR) and transmembrane domain (TM). (**D**) 293T cells were transfected to express the indicated GP subunits and mutants. 24 h.p.t. cells were harvested for WB analysis. Shown are representative WB images from $n = 2$ independent experiments. (**E**) Downregulation of surface CD81, CD63, and CD9 by EBOV GP mutants. Shown are mean values of fold of modulation (GFP−/GFP++) ±SD from $n = 3$ independent experiments.

 © The Author(s)

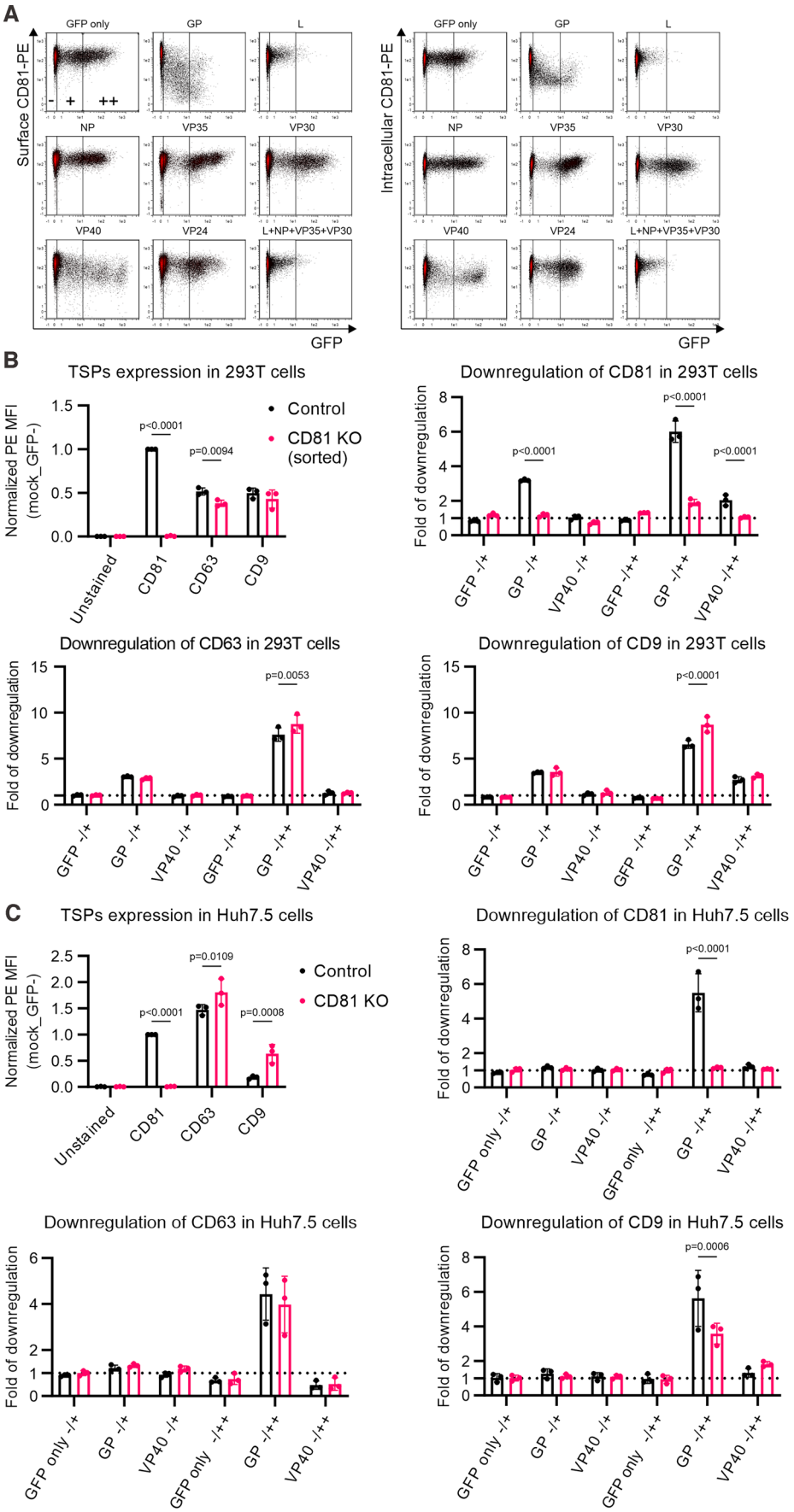
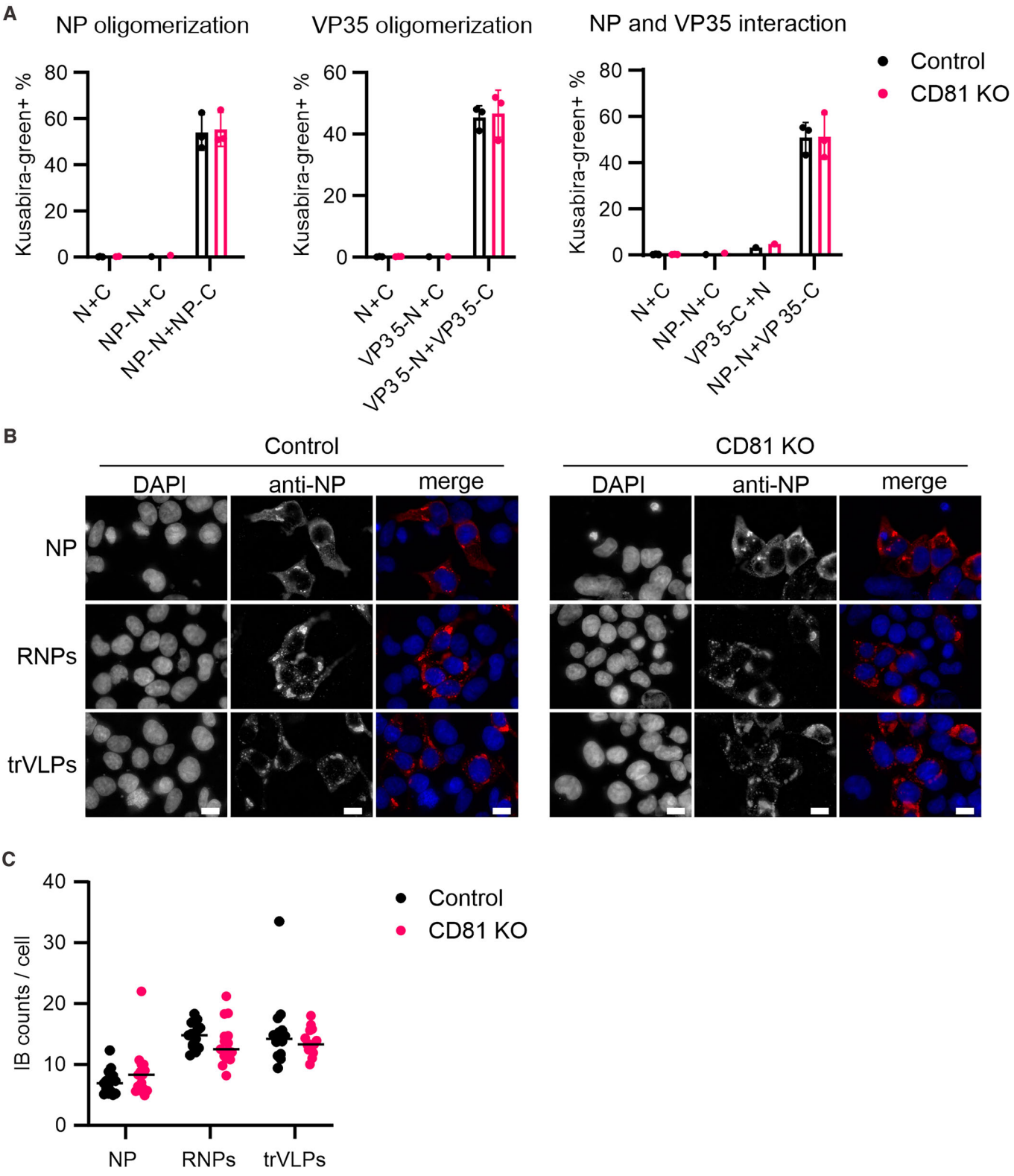

A
GFP only
GP
L
NP
VP35
VP30
VP40
VP24
L+NP+VP35+VP30
Surface CD81-PE
Intracellular CD81-PE
GFP
B
TSPs expression in 293T cells
Normalized PE MFI (mock_GFP-)
Control
CD81 KO (sorted)
p<0.0001
p=0.0094
Unstained
CD81
CD63
CD9
Downregulation of CD81 in 293T cells
Fold of downregulation
p<0.0001
GFP -/+
GP -/+
VP40 -/+
GFP -/++
GP -/++
VP40 -/++
Downregulation of CD63 in 293T cells
p=0.0053
Downregulation of CD9 in 293T cells
C
TSPs expression in Huh7.5 cells
p=0.0109
p=0.0008
CD81 KO
Downregulation of CD81 in Huh7.5 cells
GFP only -/+
GFP only -/++
Downregulation of CD63 in Huh7.5 cells
Downregulation of CD9 in Huh7.5 cells
p=0.0006

Figure EV3. Downregulation of CD63 and CD9 is not dependent on CD81.

(**A**) Modulation of surface and intracellular CD81 by EBOV proteins in 293T cells, shown are representative images of flow cytometry density plots. (**B**) 293T and (**C**) Huh7.5 cells were mock-transfected or transfected to express GFP-only or coexpress GFP and EBOV GP or VP40. 2 d.p.t., the cells were harvested and stained for CD81, CD63, and CD9 for flow cytometry analysis. Shown are mean values of normalized PE MFI (to CD81-PE MFI of mock-transfected control cells (GFP-)) and fold of modulation (in PE MFI) ± SD from $n = 3$ independent experiments. Two-way ANOVA with Šidák correction was used for statistical analysis.

© The Author(s)


A
NP oligomerization
VP35 oligomerization
NP and VP35 interaction
Kusabira-green+ %
Control
CD81 KO
N+C
NP-N+C
NP-N+NP-C
VP35-N+C
VP35-N+VP35-C
VP35-C+N
NP-N+VP35-C
B
Control
CD81 KO
DAPI
anti-NP
merge
NP
RNPs
trVLPs
C
IB counts / cell
Control
CD81 KO
NP
RNPs
trVLPs

© The Author(s)

Figure EV4. The effect of CD81 on NP and VP35 interaction and inclusion body (IB) formation.

(**A**) 293T control and CD81 KO cells were transfected to express the N- and C- part of Kusabira-green (KG) fused to N or VP35 as indicated for the BiFC assay. 2 d.p.t., the cells were harvested for flow cytometry analysis. Shown are mean values of % of KG-positive cells ± SD from $n = 3$ independent experiments. (**B**) 293T control and CD81 KO cells were transfected to express NP alone, all ribonucleoprotein (RNP) components (NP, VP35, VP30, and L), or transfected with RNPs and subsequently infected with trVLPs. Cells were fixed 24 h.p.t. and stained for NP and DAPI. Shown are representative images from $n = 3$ independent experiments. Scale bars indicate a distance of 10 μm. (**C**) The number of IBs per cell was quantified using ImageJ. Two-way ANOVA with Šidák's correction was used for statistical analysis.

 © The Author(s)

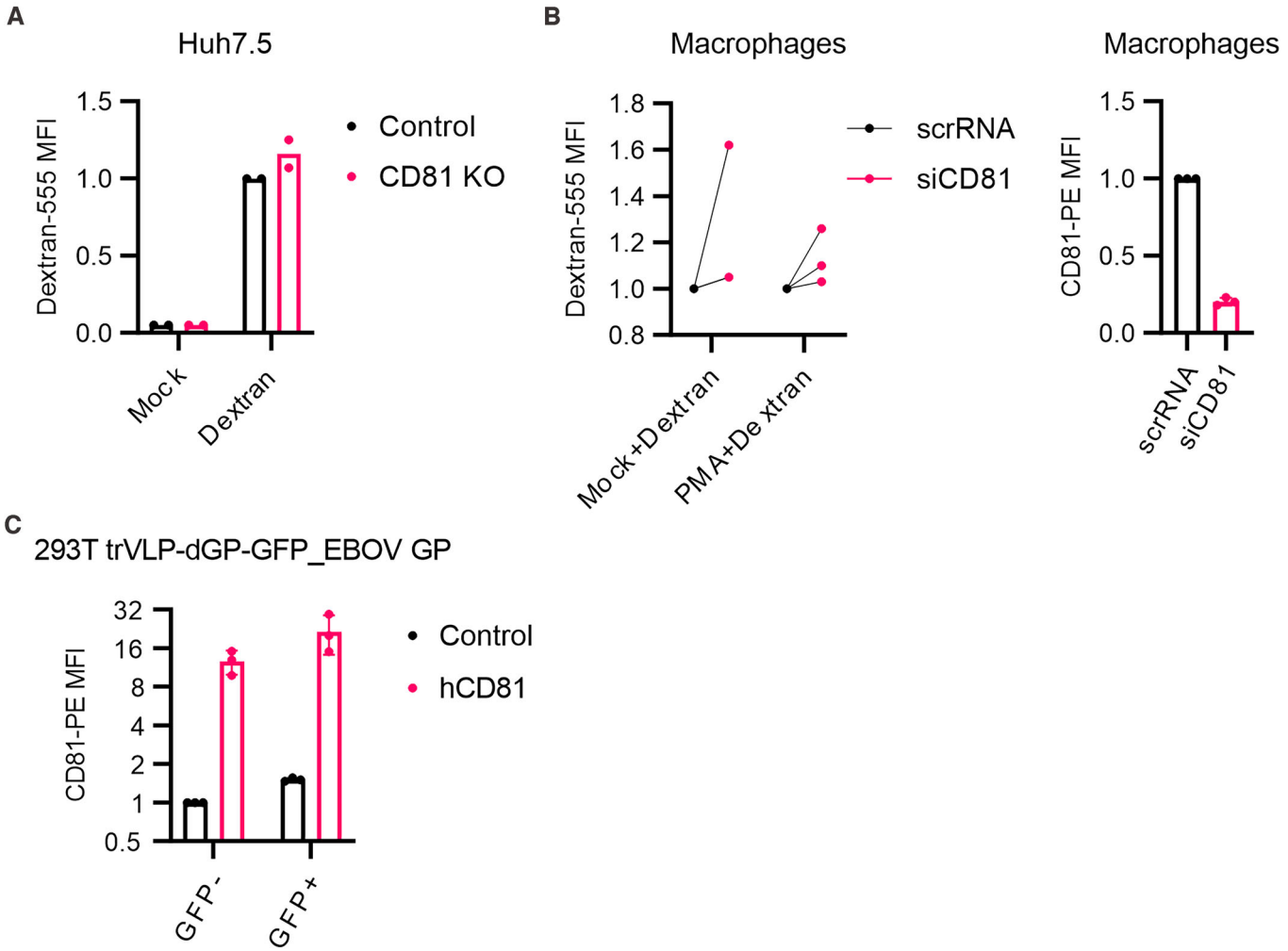


Figure EV5. The role of CD81 in EBOV trVLP infection.

(**A**) Huh7.5 control and CD81 KO cells were left untreated or incubated with Dextran-555 (10 K, 0.4 mg/ml). After incubation at 37 °C for 15 min, the cells were harvested for flow cytometry to analyze Dextran uptake. Shown are MFI values (normalized to control cells added with Dextran) ± SD from $n = 2$ independent experiments. (**B**) Human primary macrophages were transfected with non-targeting siRNA (scrRNA) or siRNA targeting CD81 (siCD81). 4 d.p.t., the cells were mock-treated or treated with PMA (1 μM). After 30 min incubation, the PMA was removed, and Dextran-555 was added. 15 min later, the cells were harvested for flow cytometry to analyze Dextran uptake. Shown is Dextran-555 MFI (normalized to scrRNA-transfected cells) of macrophages from three independent donors (left). Macrophages without PMA and Dextran-555 treatment were harvested and stained for CD81 for flow cytometry. Shown is CD81-PE MFI (normalized to scrRNA) of macrophages from the three donors. (**C**) CD81 expression of 293T cells, pre-transfected with empty vector (Empty) or human CD81 (hCD81) expression plasmid and infected with trVLP pseudotypes, was analyzed by flow cytometry. Shown are mean values of CD81-PE MFI (normalized to control non-infected (GFP-) cells) ± SD from $n = 3$ independent experiments.

© The Author(s)